

Electronic Supplementary Information (ESI)

Nucleophilic reactivity and electrocatalytic reduction of halogenated organic compounds by nickel *o*-phenylenedioxamate complexes

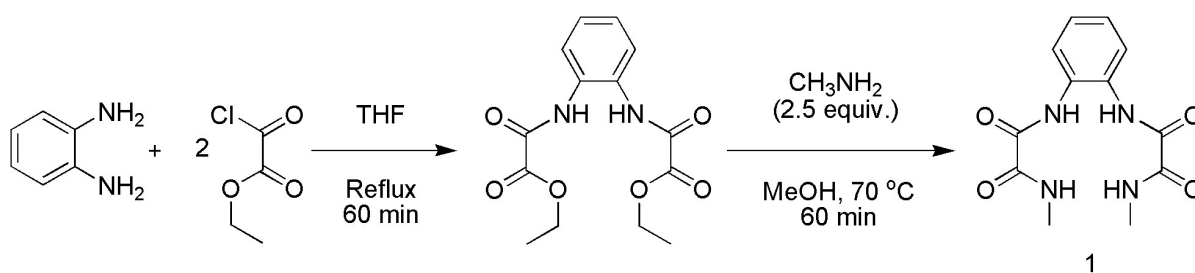
Siva Prasad Das,^a Rakesh Ganguly,^a Yongxin Li,^a and Han Sen Soo^{*,a,b,c}

^a Division of Chemistry and Biological Chemistry, School of Physical and Mathematical Sciences, Nanyang Technological University, 21 Nanyang Link 637371, Singapore. E-mail: hansen@ntu.edu.sg

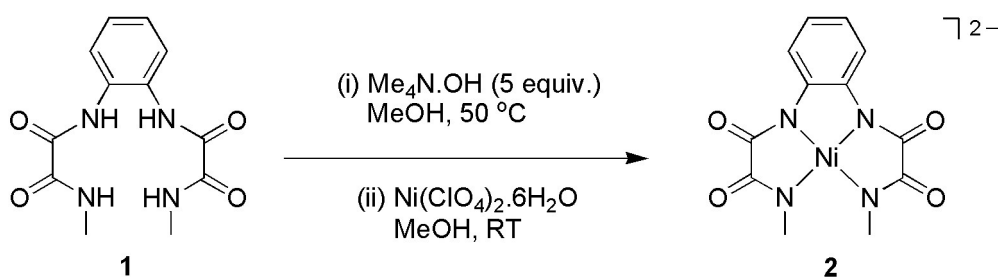
^b Singapore-Berkeley Research Initiative for Sustainable Energy (SinBeRISE), 1 Create Way, Singapore 138602.

^c Solar Fuels Laboratory, Nanyang Technological University, 50 Nanyang Avenue, Singapore 639798.

I. Synthesis



Scheme S1 Preparation of compound **1**.



Scheme S2 Preparation of compound **2**.

Compound $N^1, N^{1'}$ -(1,2-phenylene)bis(N^2 -methyloxalamide) (Me_2opba , **1**)

Compound **1** was prepared by following the procedure described previously.¹ In a typical reaction, ethyl chlorooxoacetate (1.45 mL, 13.0 mmol) were added dropwise to an *o*-phenylenediamine (0.70 g, 6.5 mmol) solution in anhydrous tetrahydrofuran (THF, 30 mL). The mixture was heated under reflux for 1 h, after which the reaction mixture was cooled to room temperature and filtered to remove any precipitate formed. The filtrate was evaporated under reduced pressure to give an oily liquid, and distilled water was added until it became a powdery solid. The solid was filtered, washed with water, and dried under reduced pressure to yield 1.53 g (4.96 mmol) of the diethyl ester precursor. The white powdery diethyl ester precursor thus obtained was dissolved in methanol (15 mL). Subsequently, a 40%

methylamine solution (1.00 mL, 12.4 mmol) in methanol was added to the solution of the diethyl ester precursor and the reaction mixture was heated at 70 °C for 1 h. The reaction mixture was cooled to room temperature, filtered, and washed with methanol and diethyl ether before being dried *in vacuo* to yield pure **1** (1.33 g, 4.78 mmol). The product identity has been confirmed by NMR spectroscopy and HR-ESI-MS. ¹H NMR (DMSO-*d*₆, 300 MHz): δ = 2.74 (d, *J* = 3.0 Hz, 6 H), 7.28 (dd, *J* = 3.6, 6.0 Hz, 2 H), 7.61 (dd, *J* = 3.6, 6.0 Hz, 2 H), 8.96 (d, *J* = 3.0 Hz, 2 H), 10.47 (s, 2 H). ¹³C{¹H} NMR (DMSO-*d*₆, 75 MHz): δ = 26.0, 125.4, 126.1, 129.9, 158.6, 160.0. HRMS (ESI+, *m/z*) calculated for C₁₂H₁₅N₄O₄ [M + H]⁺ *m/z* = 279.1093, found 279.1096.

Reaction of 2 with iodoethane to form 3b:

Complex **3b** was synthesized by following the method as mentioned for **3a**. Instead of iodomethane for **3a**, iodoethane (0.071 g, 0.45 mmol) was used. Yield = 0.031 g (77.8%). Suitable single crystals for X-ray structural analysis were grown from diffusion of anhydrous diethyl ether into a MeCN solution of the complex. ¹H NMR (CD₃CN, 300 MHz): δ = 1.32 (t, 6.9 Hz, 3 H), 2.51 (s, 3 H), 2.80 (s, 3 H), 3.08 (s, 12 H), 4.88 (q, 6.9 Hz, 2 H), 6.59-6.71 (m, 2 H), 7.97 (dd, *J* = Hz, 1 H), 8.07 (dd, *J* = Hz, 1 H). ¹³C{¹H} NMR (CD₃CN, 75 MHz): δ = 16.3, 32.9, 36.0, 56.2 (t), 69.2, 119.6, 120.0, 121.8, 123.5, 142.9, 145.9, 160.0, 163.8, 165.8, 171.3. HRMS (ESI-, *m/z*) calculated for C₁₄H₁₅N₄NiO₄ [M]⁻ *m/z* = 361.0447, found 361.0455. Elemental analyses for C₁₈H₂₇N₅NiO₄ calculated: C, 49.57; H, 6.24; N, 16.06%; found: C, 49.38; H, 6.31; N, 15.83%.

Reaction of 2 with 2-iodopropane to form 3c:

The complex **3c** was synthesized by following the method described for **3a**. In this reaction, 2-iodopropane (0.077 g, 0.45 mmol) was used. Yield = 0.035 g (88.9%). Diffusion of anhydrous diethyl ether into a MeCN solution of the complex at 5 °C gave red crystals that were suitable for single crystal X-ray structural analysis. ¹H NMR (CD₃CN, 300 MHz): δ = 1.32 (d, J = 6.3 Hz, 6 H), 2.51 (s, 3 H), 2.80 (s, 3 H), 3.09 (s, 12 H), 6.08 (sep, J = 6.3 Hz, 1 H), 6.59-6.71 (m, 2 H), 7.97 (dd, J = 1.5, 7.8 Hz, 1 H), 8.06 (dd, J = 1.5, 7.8 Hz, 1 H). ¹³C{¹H} NMR (CD₃CN, 75 MHz): δ = 23.6, 32.8, 36.2, 56.2 (t), 76.5, 119.6, 120.0, 121.6, 123.6, 142.9, 146.0, 160.0, 164.1, 165.8, 171.3. HRMS (ESI⁻, m/z) calculated for C₁₅H₁₇N₄NiO₄ [M]⁻ m/z = 375.0603, found 375.0611. Elemental analyses for C₁₉H₂₉N₅NiO₄ calculated: C, 50.69; H, 6.49; N, 15.56%; found: C, 50.75; H, 6.53; N, 15.49%.

Reaction of 2 with 1-iodo-2-methylpropane to form 3d:

Complex **3d** was synthesized by following the procedure described for **3a** with modifications to the reaction conditions. The reaction was carried out at 45 °C for five days. In this reaction, 1-iodo-2-methylpropane (0.083 g, 0.45 mmol) was used. Yield = 0.012 g (28.7%). Suitable single crystals for X-ray structural analysis were grown from diffusion of anhydrous diethyl ether into a MeCN solution of the complex at 5 °C. ¹H NMR (CD₃CN, 500 MHz): δ = 0.97 (d, J = 6.5 Hz, 6 H), 1.96 (m, 1 H), 2.51 (s, 3 H), 2.81 (s, 3 H), 3.09 (s, 12 H), 4.64 (d, J = 6.5 Hz, 2 H), 6.62 (td, J = 1.5, 8.0 Hz, 1 H), 6.69 (td, J = 1.5, 8.0 Hz, 1 H), 7.96 (dd, J = 1.5, 7.8 Hz, 1 H), 8.06 (dd, J = 1.5, 7.8 Hz, 1 H). ¹³C{¹H} NMR (CD₃CN, 75 MHz): δ = 19.0 (2 C), 30.1, 32.8, 36.0, 56.3 (t), 78.8, 119.7, 119.9, 121.7, 123.6, 142.9, 146.0, 160.0, 163.7, 165.8, 171.3. HRMS (ESI⁻, m/z) calculated for C₁₆H₁₉N₄NiO₄ [M]⁻ m/z = 389.0760, found 389.0765. Elemental analyses for C₂₀H₃₁N₅NiO₄ calculated: C, 51.75; H, 6.73; N, 15.09%; found: C, 51.77; H, 6.95; N, 14.70%.

Reaction of **2** with bromoethane to form **3b**:

The reaction of **2** with bromoethane was carried out in a J. Young NMR tube at 60 °C. In a typical reaction, bromoethane (0.98 mg, 0.0090 mmol) was added to a solution of **2** (1.00 mg, 0.0018 mmol) in CD₃CN (1.0 mL). The NMR tube was heated at 60 °C and the progress was monitored by ¹H NMR spectroscopy at different time intervals. The ¹H NMR spectra recorded at different times are shown in Fig. S13. It was found that new signals appeared in the regions of $\delta = \sim 7.8$, ~ 6.6 , ~ 4.8 , ~ 2.8 , and ~ 1.3 ppm, which are characteristic peaks for the ethylated **2** (traces b, c, and d of Fig. S13). Beside these, the ESI-MS recorded for the reaction mixture showed peaks at $m/z = 361.04$, which corresponded to [**3b**]⁻. These observations clearly suggest that bromoethane reacted with **2** and formed product **3b**. However, the reaction of **2** with bromoethane was found to be slower than that with iodoethane. We have not isolated the **3b** formed in this reaction of **2** with bromoethane from the reaction mixture.

Reaction of **2** with 2-bromopropane to form **3c**:

The reaction of **2** with 2-bromopropane was conducted in a J. Young NMR tube under identical reaction conditions as mentioned above for the reaction of **2** with bromoethane. In this reaction, 2-bromopropane (1.11 mg, 0.0090 mmol) was used. The ¹H NMR spectra recorded at different times are shown in Fig. S14. It was found that new signals appeared in the regions of $\delta = \sim 7.8$, ~ 6.6 , ~ 6.1 , ~ 2.8 , and ~ 1.3 ppm, which are characteristic peaks for iso-propylated **2** (traces b, c, and d of Fig. S14). In addition, the ESI-MS recorded for the reaction mixture showed peaks at $m/z = 374.85$, which corresponded to [**3c**]⁻. These observations clearly suggest that 2-bromopropane reacted with **2** and formed product **3c**.

However, the reaction of **2** with 2-bromopropane was found to be much slower than that with 2-iodopropane. Likewise, we have not isolated the **3c** formed by reaction of **2** with 2-bromopropane from the reaction mixture.

Reaction of 2 with 2-bromoethanol, with possible product 3e:

The reaction of **2** with 2-bromoethanol was carried out in a J. Young NMR tube by following the procedure described above for the reaction of **2** with bromoethane with modifications to the reaction temperature. The reaction was conducted at 0 °C. In a typical reaction, 2-bromoethanol (1.79 mg, 0.0090 mmol) was used as substrate. The ¹H NMR spectra recorded at different times are shown in Fig. S15. It was found that new signals appeared in the regions of $\delta = \sim 7.8$, ~ 6.6 , and ~ 2.8 ppm, which were characteristic peaks for alkylated **2** (traces b, c and d of Fig. S15). These observations clearly suggest that 2-bromoethanol reacted with **2** and formed a new product **3e**. However, the conversion for the reaction was very low and we could not isolate pure **3e** from the reaction mixture. After prolonged reaction periods (7 days), the product decomposed and Ni(II) dissociated from the complex (trace e of Fig. S15). Multiple attempts to obtain single crystals of **3e** for X-ray diffraction analysis have not been successful so far.

Reaction of 2 with bromotrichloromethane to form possible product 3f:

The reaction of **2** with bromotrichloromethane was carried out by adopting a similar procedure as described for bromoethane. In this reaction, bromotrichloromethane (1.13 mg, 0.0090 mmol) was used instead and the reaction was conducted at 0 °C. The initial yellow color of **2** turned brown within 4 h. The ¹H NMR spectra of the reaction mixture have been recorded at different times and are shown in Fig. S16. The signals for **2** disappeared within 10 min, indicating that **2** was consumed. The absence of any new resulting peaks within a window of -100 to +100 ppm suggested that BrCCl₃ oxidized **2** to give paramagnetic and NMR-silent Ni(III) product(s). Multiple attempts to isolate single crystals that are suitable for X-ray diffraction have not been successful so far. In addition, our attempts to trap the •CCl₃ radical with the help of EPR spectroscopy at room temperature have also been unsuccessful due to its high reactivity. Beside these, we were unable to observe C₂Cl₆ in the reaction mixture by GC-MS.

Reaction of **2 with benzyl bromide to form possible product **3g**:**

The reaction of **2** with benzyl bromide was carried out by adopting a slightly modified procedure as described for bromoethane. Typically, each reaction was carried out at room temperature using benzyl bromide (1.54 mg, 0.0090 mmol) as the substrate. The initially yellow colored reaction mixture turned slightly red after 72 h. The ¹H NMR spectra of the reaction mixture recorded at different time intervals are shown in Fig. S17. It was found that new signals appeared in the regions of $\delta = \sim 7.8$, ~ 6.6 , and ~ 2.8 ppm, which were characteristic peaks for alkylated **2** (traces b, c and d of Fig. S17). These observations clearly suggest that benzyl bromide reacted with **2** and formed at least one new product **3g**. However, the conversion for the reaction was very low and we could not isolate pure **3g** from the reaction mixture. Furthermore, as a side reaction, the product decomposed and Ni(II)

dissociated from the complex since the beginning of the reaction to form the hydrolyzed ligand **1** (trace b of Fig. S17).

Reaction of **2 with pentafluoropyridine to form possible product **3h**:**

The reaction of **2** with pentafluoropyridine was carried out by adopting the procedure as mentioned above for **3g**. The reaction was carried out at room temperature using pentafluoropyridine (1.52 mg, 0.0090 mmol) as the substrate. The ^1H NMR spectra of the reaction mixture recorded at different time intervals are shown in Figure S18. It was found that new signals appeared in the regions of $\delta = \sim 7.8$, ~ 6.6 , and ~ 2.8 ppm, which were characteristic peaks for alkylated **2** (traces b, c and d of Fig. S18). Additionally, the $^{19}\text{F}\{^1\text{H}\}$ NMR spectrum of the reaction mixture recorded after 36 h showed a new peak at -174.7 ppm (Fig. S19). These observations clearly suggest that pentafluoropyridine reacted with **2** and formed at least one new product **3h**. However, we could not definitively isolate and identify the pure product from the reaction mixture.

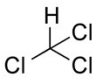
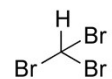
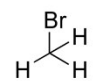
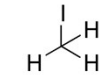
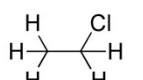
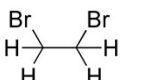
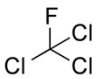
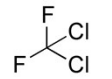
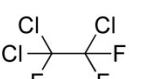
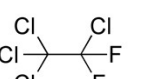
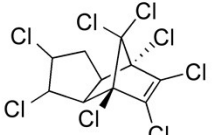
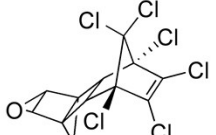
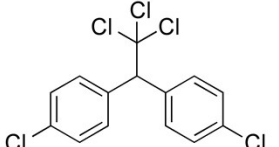
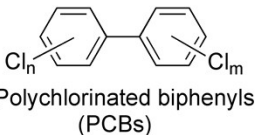
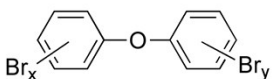
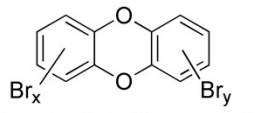
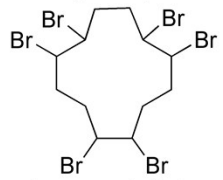
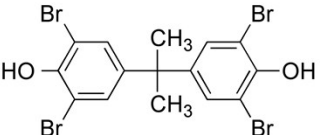
Compound / Structure	Uses	Compound / Structure	Uses
 Chloroform	Precursor of Teflon Solvent	 Bromoform	Solvent Flame retardant
 Bromomethane	Fumigant	 Iodomethane	Fumigant
 Chloroethane	Blowing agent Solvent	 Dibromoethane	Fumigant
 Trichlorofluoromethane (CFC-11)	Refrigerant	 Dichlorodifluoromethane (CFC-12)	Refrigerant
 1,1,2-trichloro-1,2,2-trifluoroethane (CFC-113)	Refrigerant	 Chloropentafluoroethane (CFC-115)	Refrigerant
 Chlordane	Insecticide	 Aldrin/Dieldrin	Insecticide
 Dichlorodiphenyltrichloroethane (DDT)	Insecticide	 Polychlorinated biphenyls (PCBs)	Heat exchange fluids Paint additives
 Polybrominated diphenyl ether (PBDE)	Flame retardant	 Polybrominated dibenzo-p-dioxin (PBDD)	Flame retardant
 Hexabromocyclododecane (HBCD)	Flame retardant	 Tetrabromobisphenol A (TBBPA)	Flame retardant

Chart S1 Examples of some common halogenated organic pollutants listed in the US Environmental Protection Agency (EPA) priority list of pollutants and in the European Commission list of priority substances.

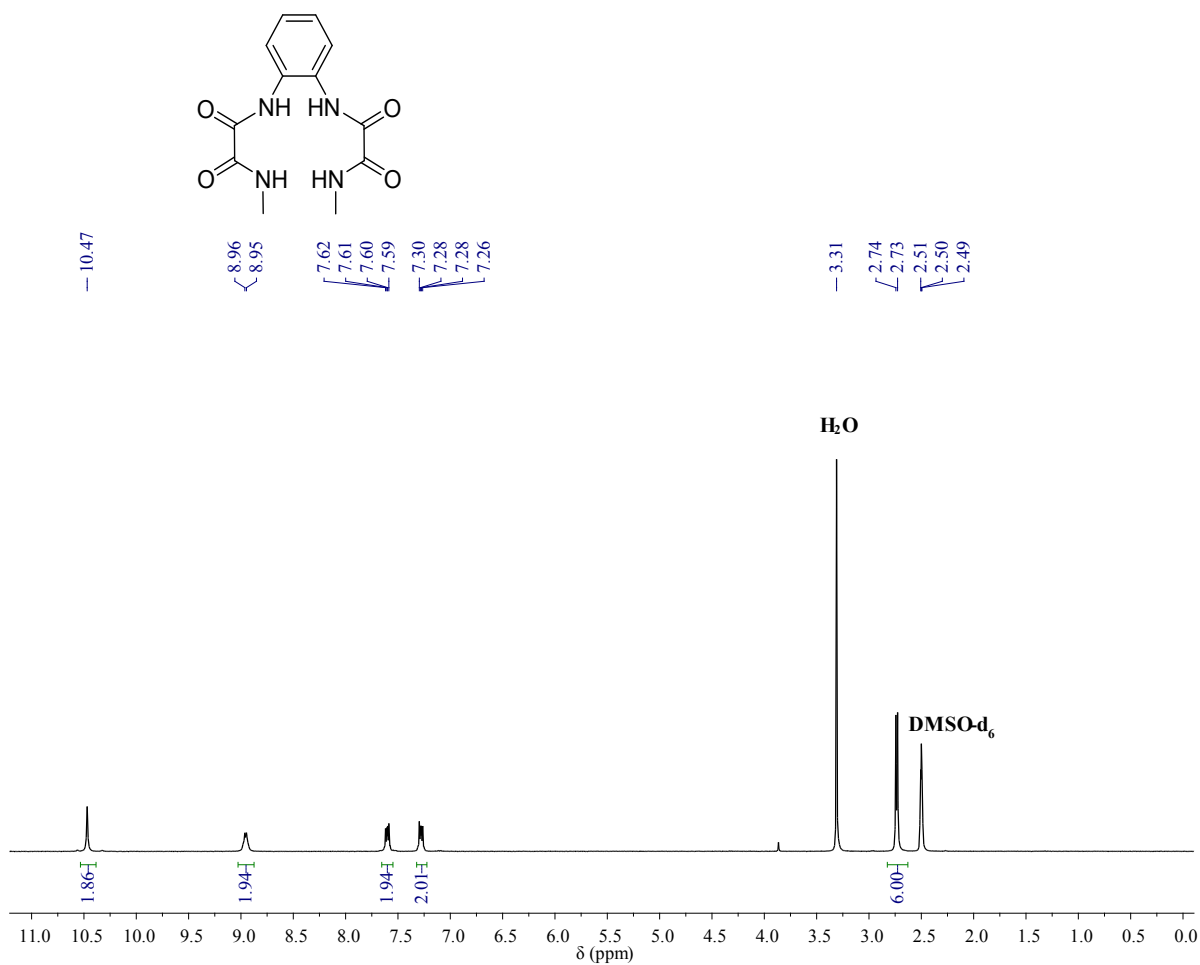


Fig. S1 The ¹H NMR spectrum of compound **1** in DMSO-*d*₆.

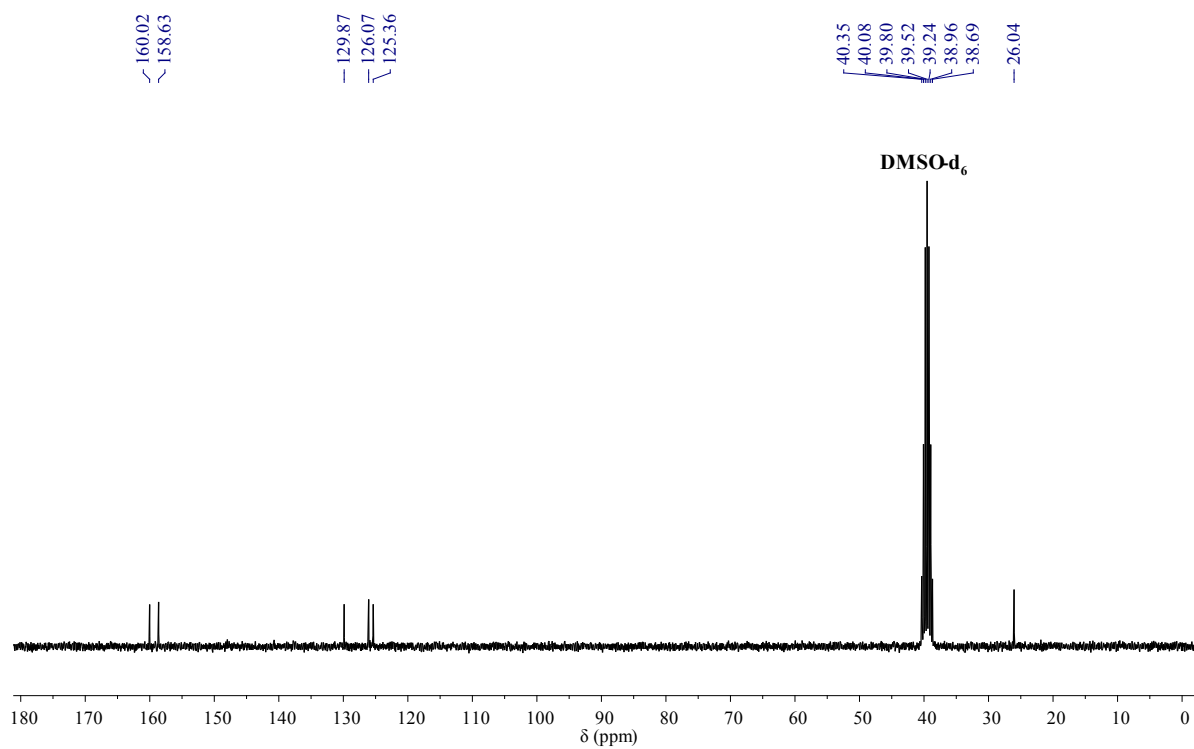


Fig. S2 The ¹³C NMR spectrum of compound **1** in DMSO-*d*₆.

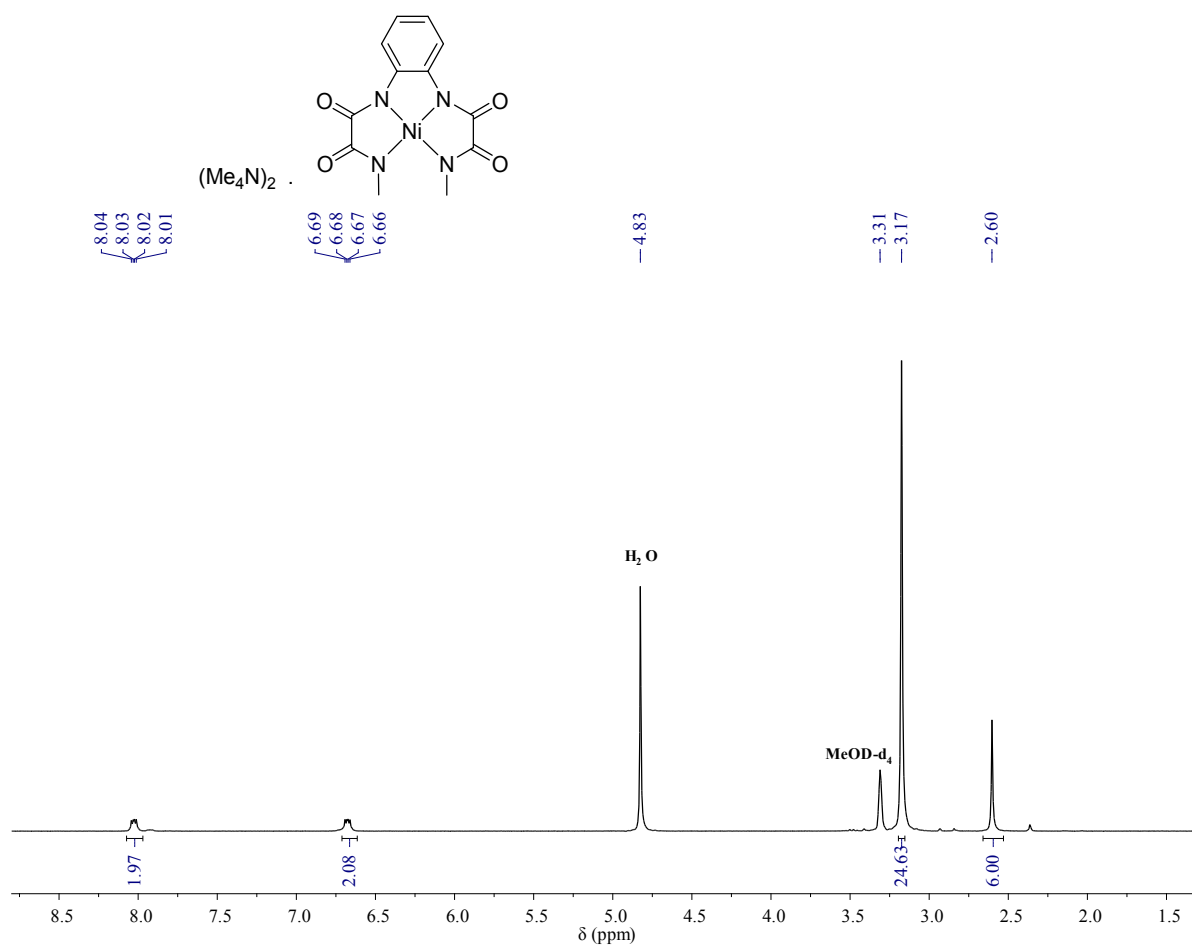


Fig. S3 The ^1H NMR spectrum of compound 2 in $\text{MeOD-}d_4$.

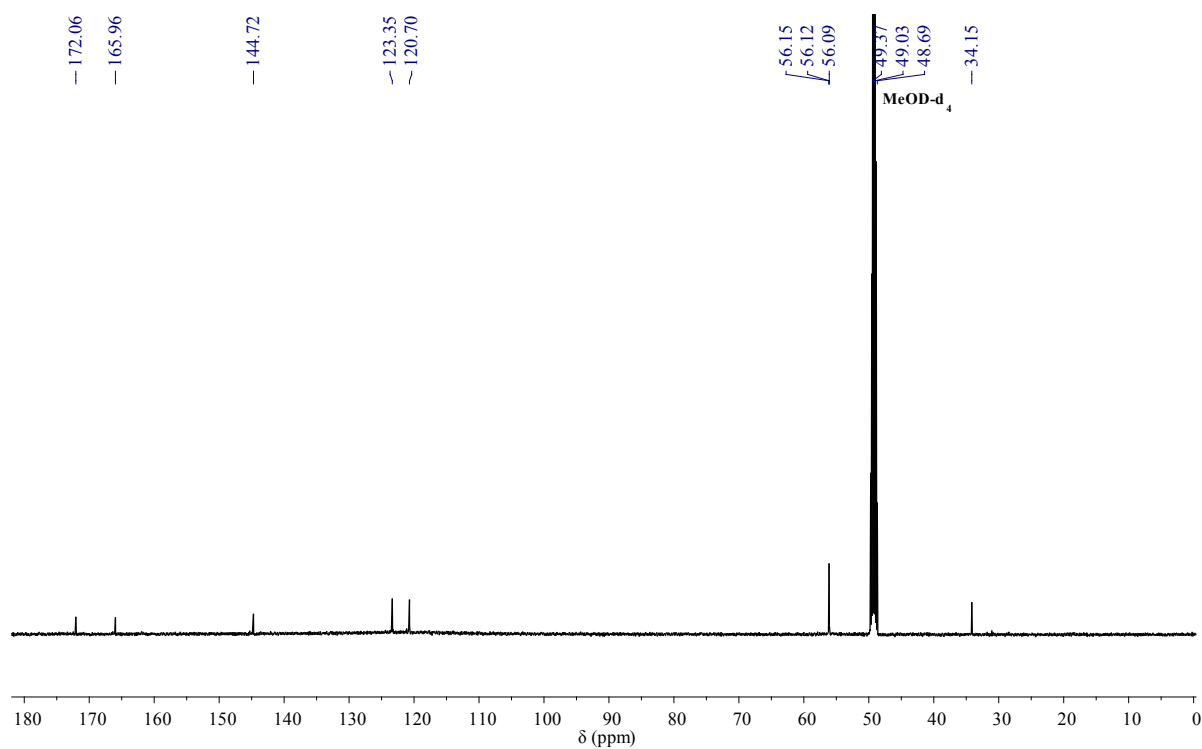


Fig. S4 The ^{13}C NMR spectrum of compound 2 in $\text{MeOD-}d_4$.

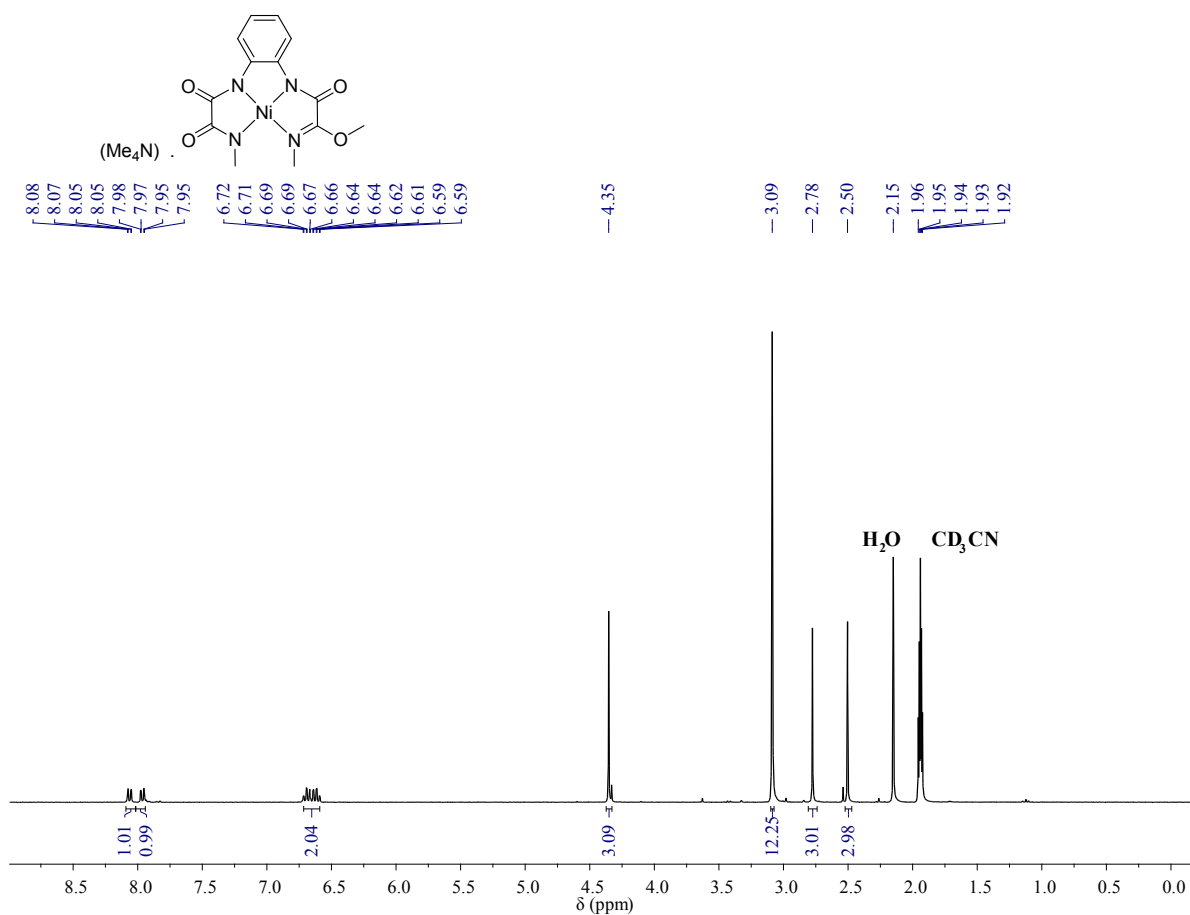


Fig. S5 The ^1H NMR spectrum of compound **3a** in CD_3CN .

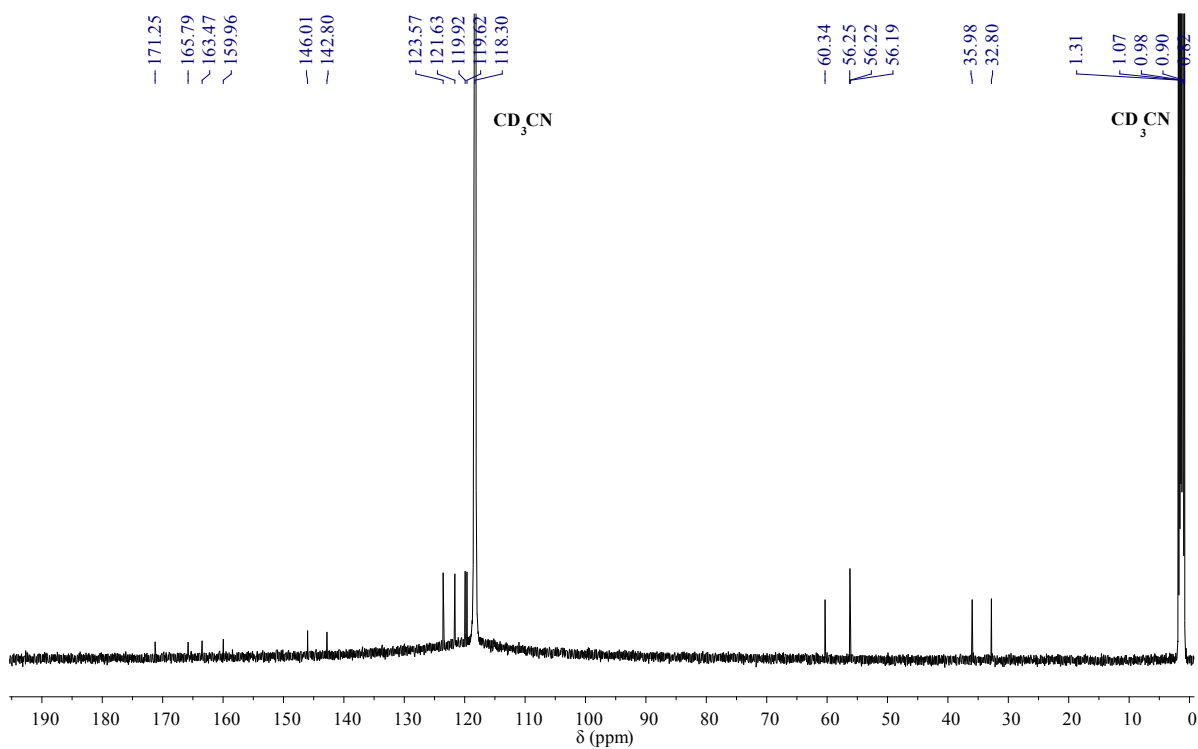


Fig. S6 The ^{13}C NMR spectrum of compound **3a** in CD_3CN .

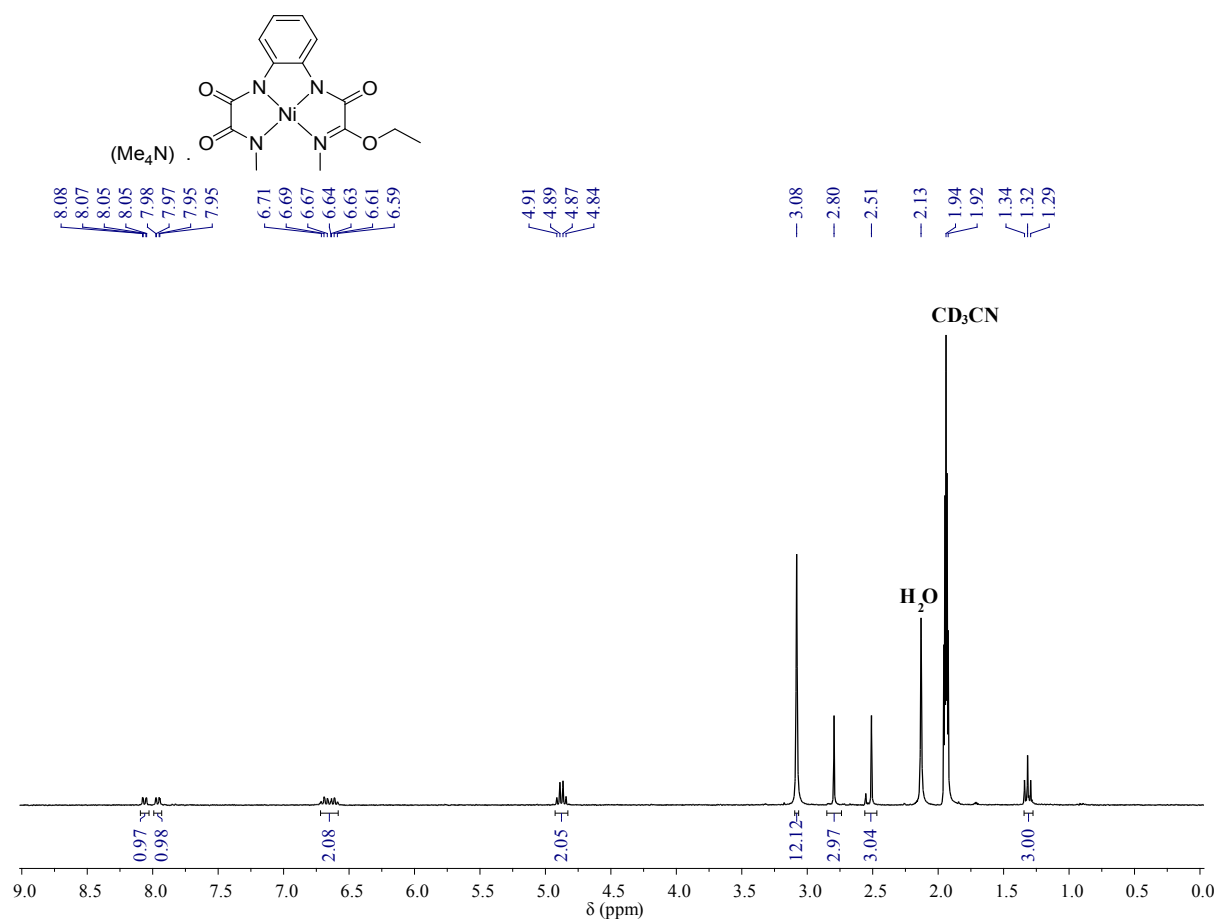


Fig. S7 The ^1H NMR spectrum of compound **3b** in CD_3CN .

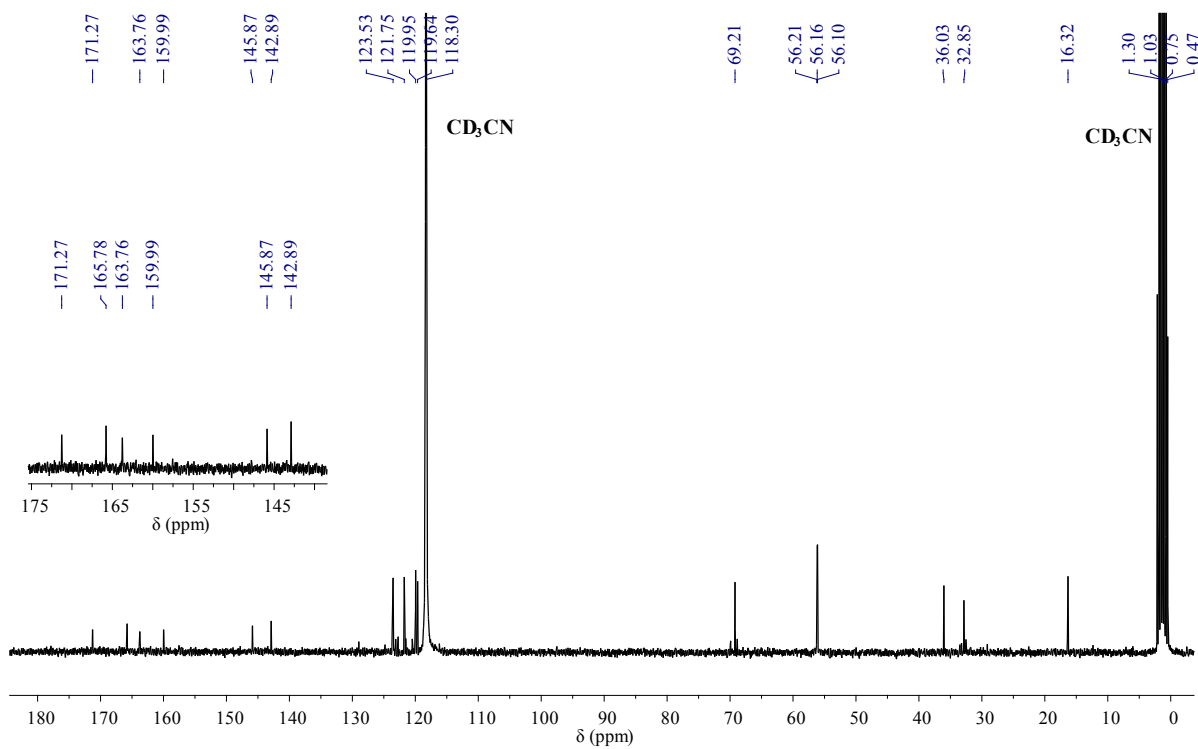


Fig. S8 The ^{13}C NMR spectrum of compound **3b** in CD_3CN .

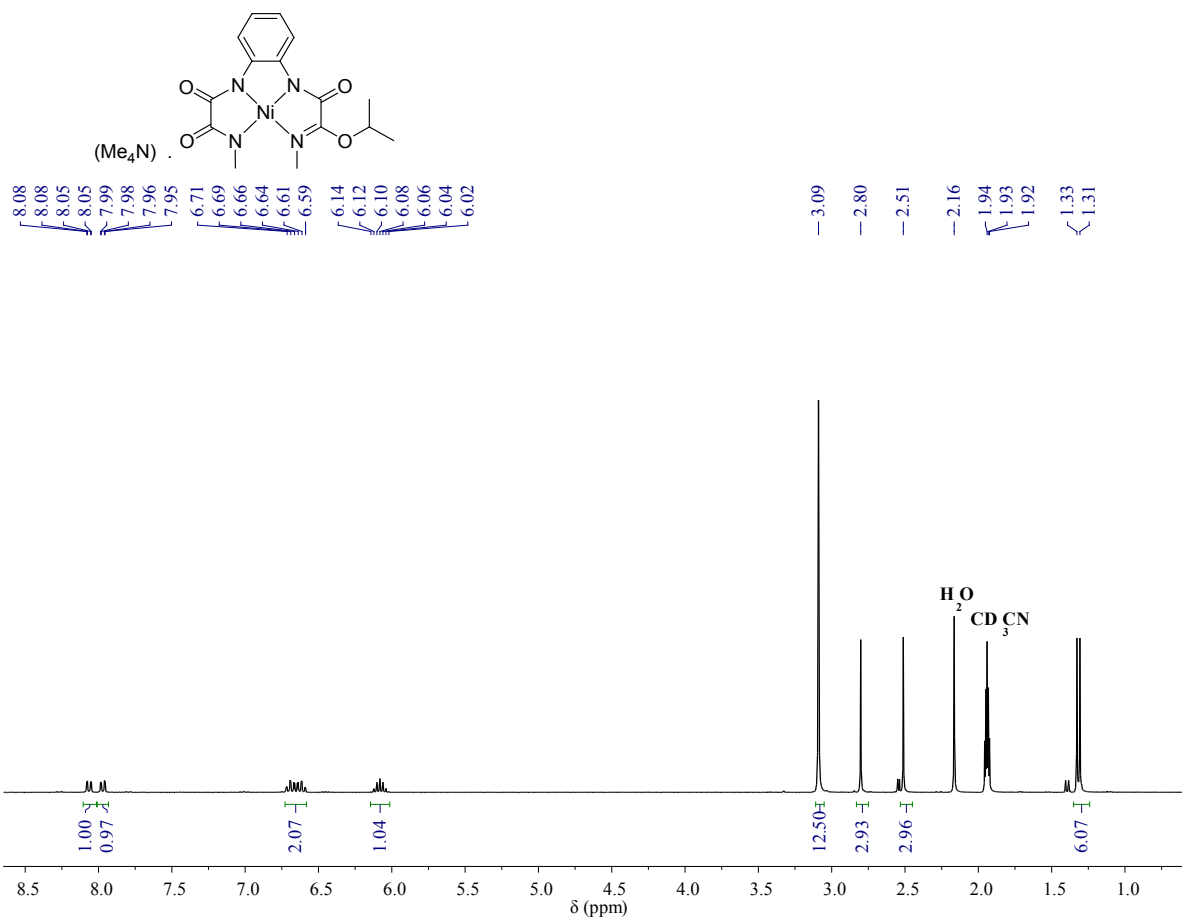


Fig. S9 The ¹H NMR spectrum of compound **3c** in CD₃CN.

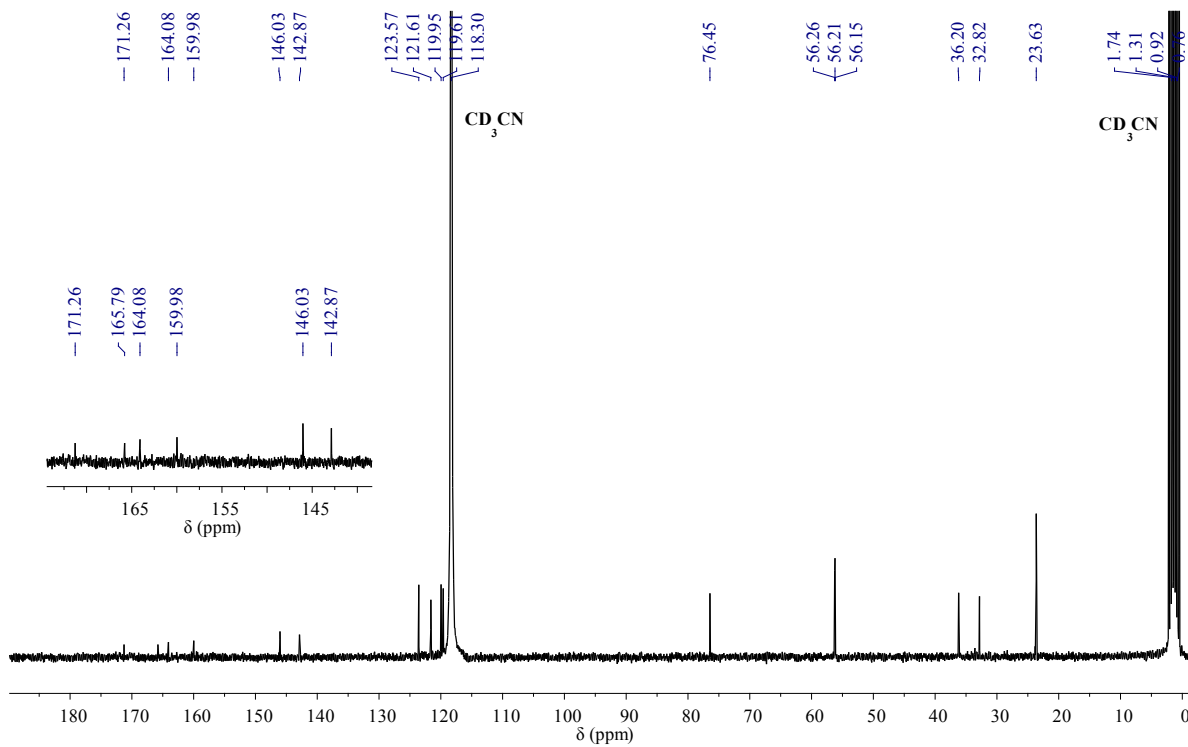


Fig. S10 The ¹³C NMR spectrum of compound **3c** in CD₃CN.

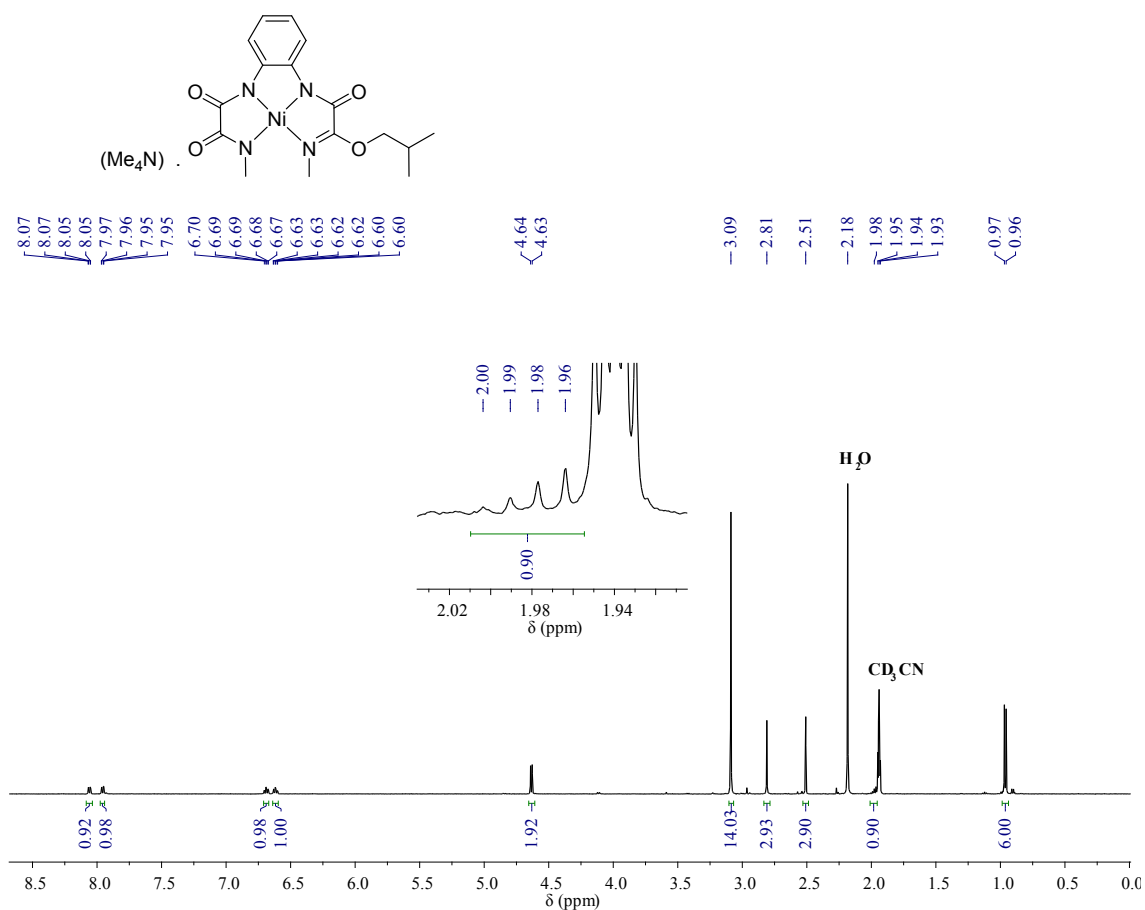


Fig. S11 The ¹H NMR spectrum of compound **3d** in CD₃CN.

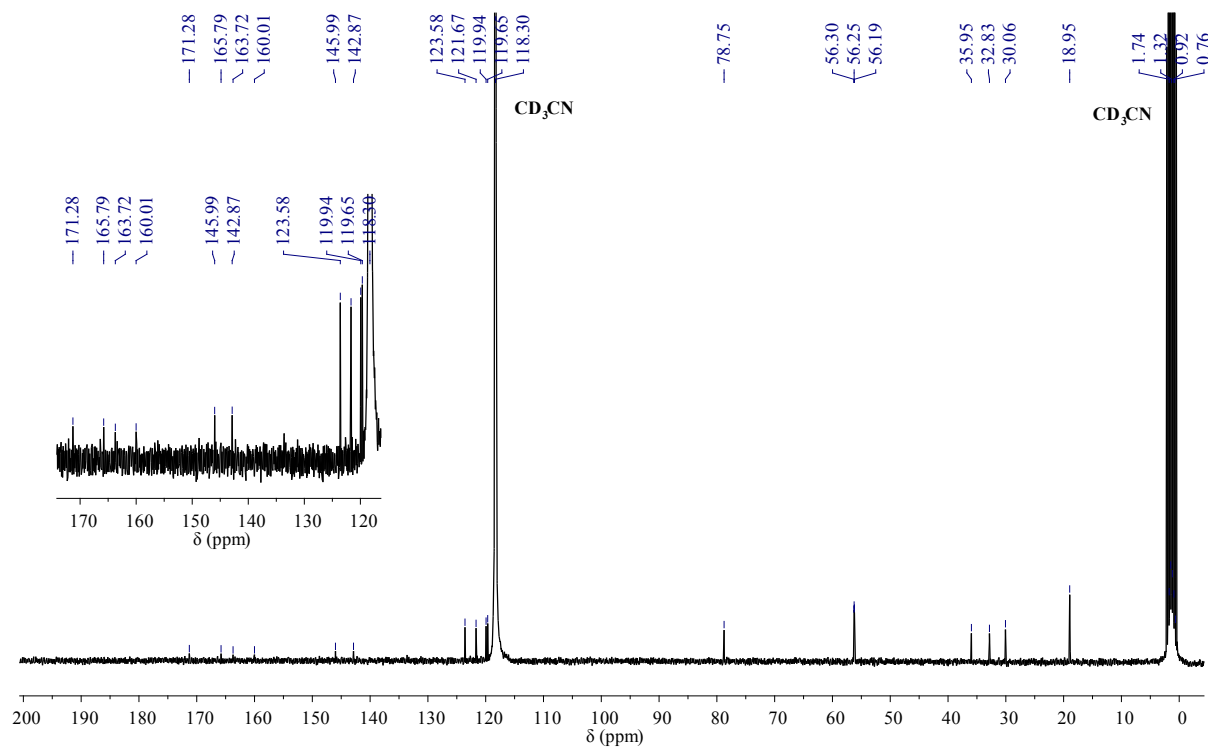


Fig. S12 The ¹³C NMR spectrum of compound **3d** in CD₃CN.

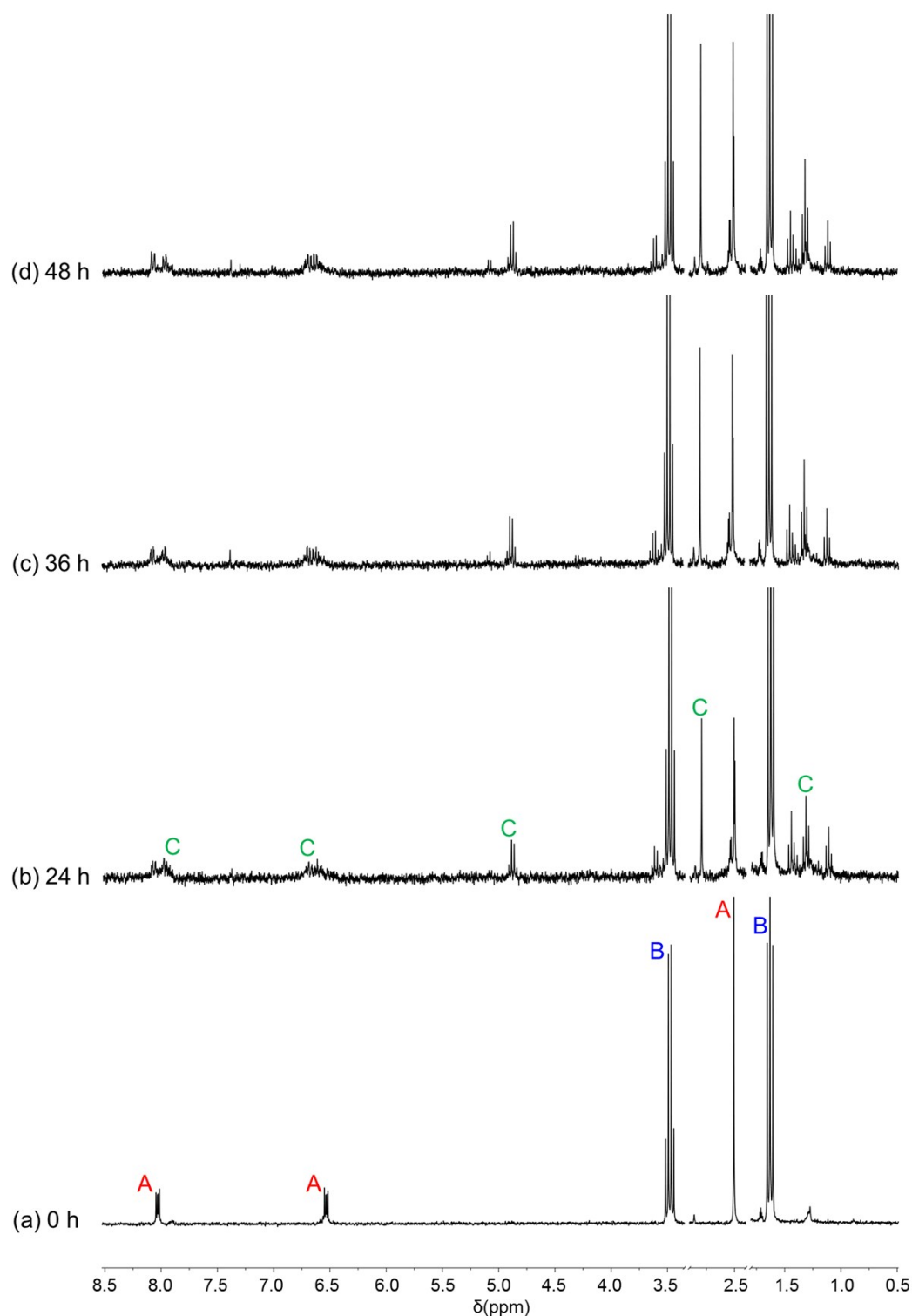


Fig. S13 The ^1H NMR spectra for the reaction of **2** with bromoethane in CD_3CN at different reaction times (a) 0 h, (b) 24 h, (c) 36 h, and (d) 48 h. In the spectra, A = **2**, B = bromoethane, C = new peaks for **3b**. The segments from $\delta = 1.80$ to 2.40 , and 2.90 to 3.35 , have been omitted because they show little relevant data. Reaction conditions: **2** = 1.00 mg, 0.0018 mmol; bromoethane = 0.97 mg, 0.0090 mmol; CD_3CN = 1.00 mL; reaction temperature = 60 $^\circ\text{C}$.

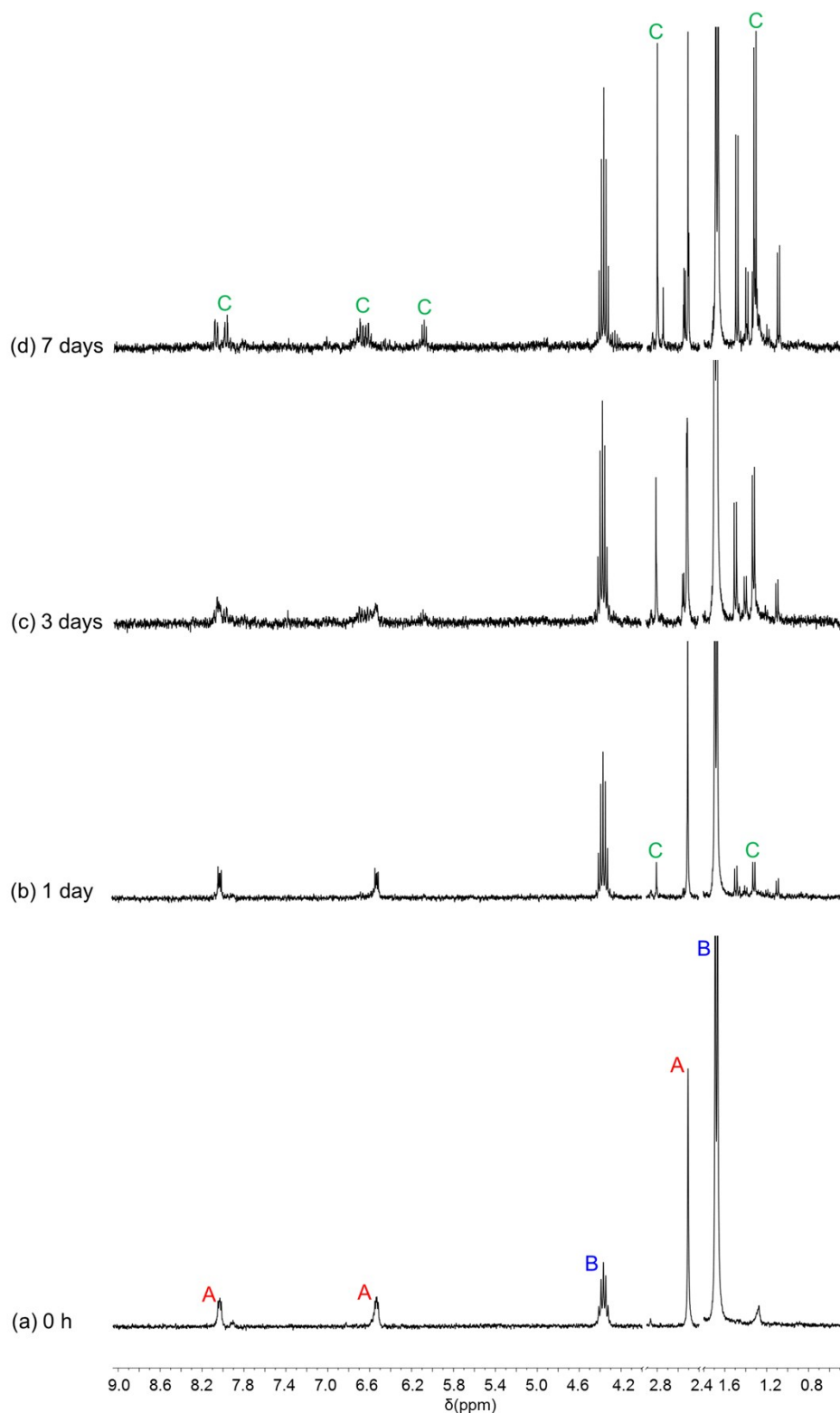


Fig. S14 The ^1H NMR spectra for the reaction of **2** with 2-bromopropane in CD_3CN at different reaction times (a) 0 h, (b) 1 day, (c) 3 days, and (d) 7 days. In the spectra, A = **2**, B = 2-bromopropane, and C = new peaks for **3c**. The segments from $\delta = 1.80$ to 2.40 , and 2.90 to 4.00 , have been omitted because they show little relevant data. Reaction conditions: **2** = 1.00 mg, 0.0018 mmol; 2-bromopropane = 1.11 mg, 0.0090 mmol; CD_3CN = 1.00 mL; reaction temperature = $60\text{ }^\circ\text{C}$.

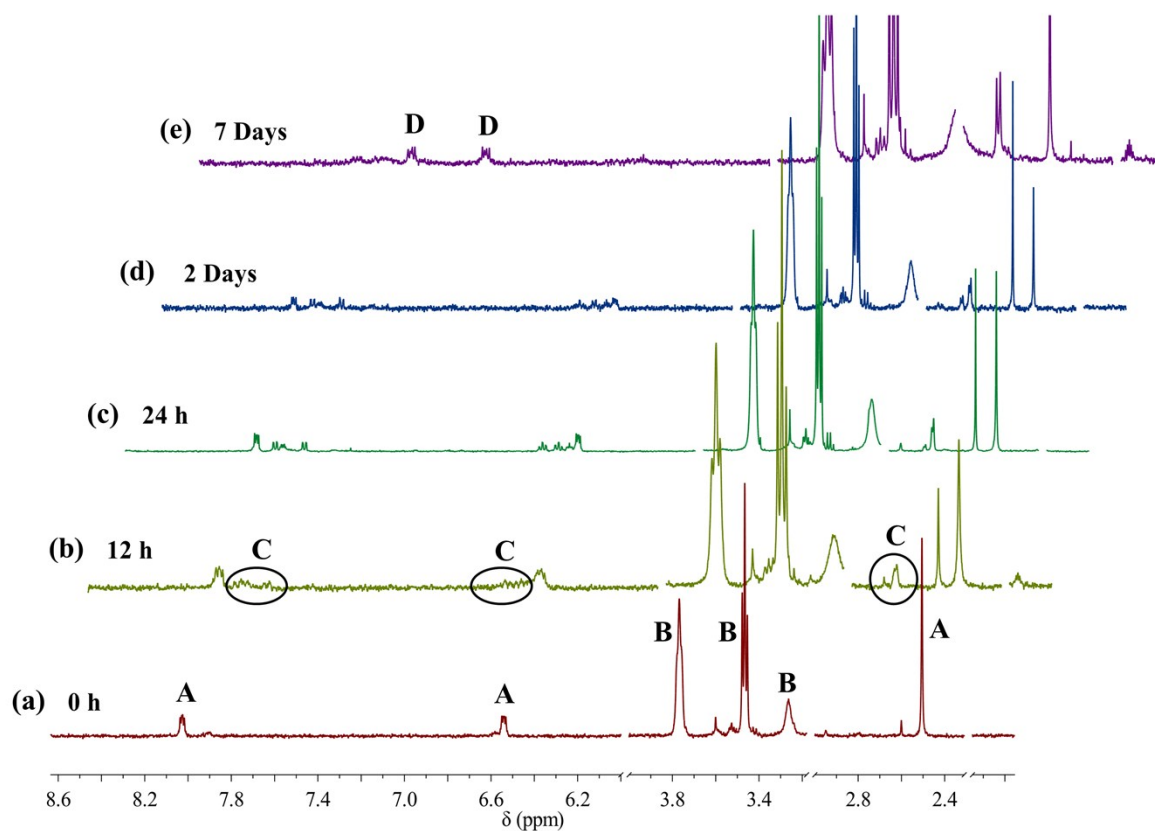


Fig. S15 The ¹H NMR spectra for the reaction of **2** with 2-bromoethanol in CD₃CN at different reaction times. In the spectra, A = **2**, B = 2-bromoethanol, C = new peaks for **3e** and D = **1**. The segments from $\delta = 1.75$ to 2.31, 3.00 to 3.18, and 4.00 to 6.00, have been omitted because they show little relevant data. Reaction conditions: **2** = 1.00 mg, 0.0018 mmol; 2-bromoethanol = 1.79 mg, 0.0090 mmol; CD₃CN = 1.00 mL; reaction temperature = 0 °C.

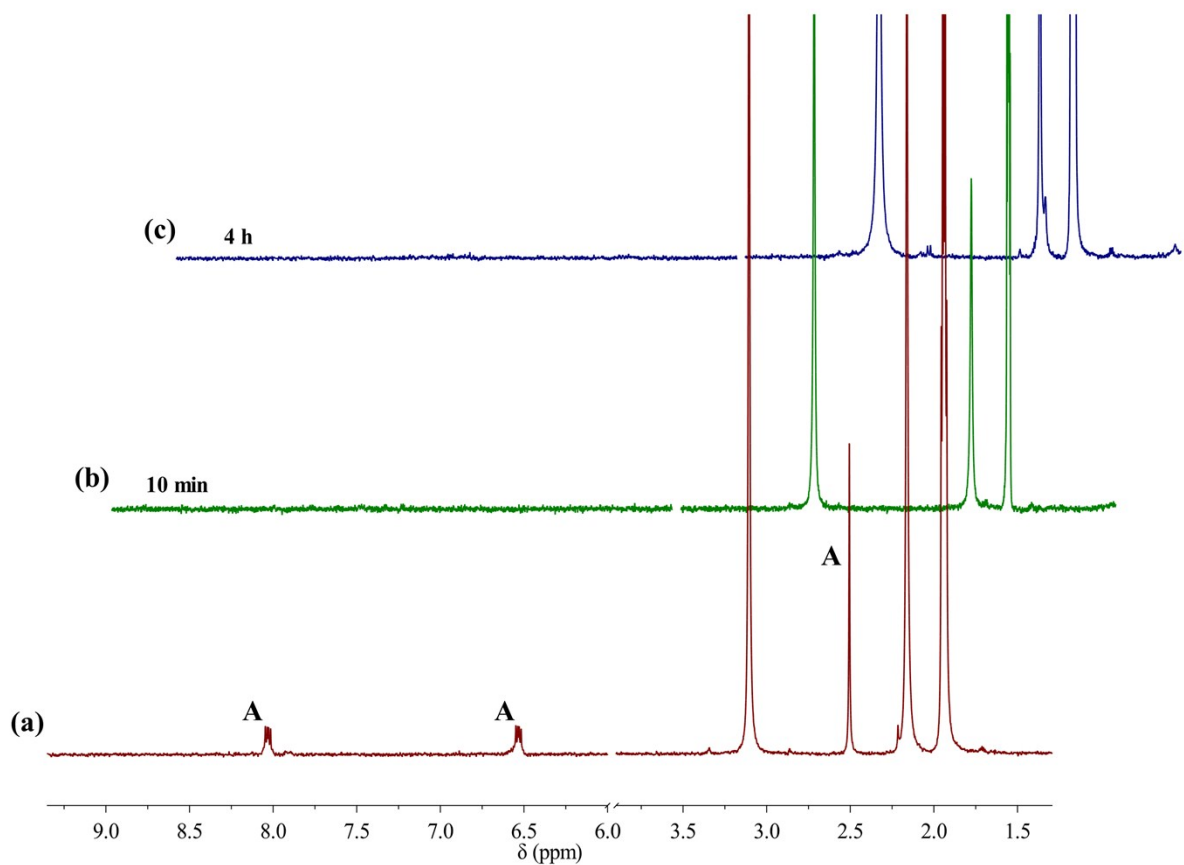


Fig. S16 The ¹H NMR spectra for the reaction of **2** with bromotrichloromethane (BrCCl₃) in CD₃CN at different reaction times. In the spectra, A = complex **2**. The spectra correspond to the reaction mixture (a) before addition of BrCCl₃, (b) 10 min after addition of BrCCl₃, and (c) 4 h after spectrum (b) was collected. The segment from $\delta = 4.00$ to 6.00 has been omitted since it shows a flat line with no relevant data. Reaction conditions: **2** = 1.00 mg, 0.0018 mmol; BrCCl₃ = 1.13 mg, 0.0090 mmol; CD₃CN = 1.00 mL; reaction temperature = 0 °C.

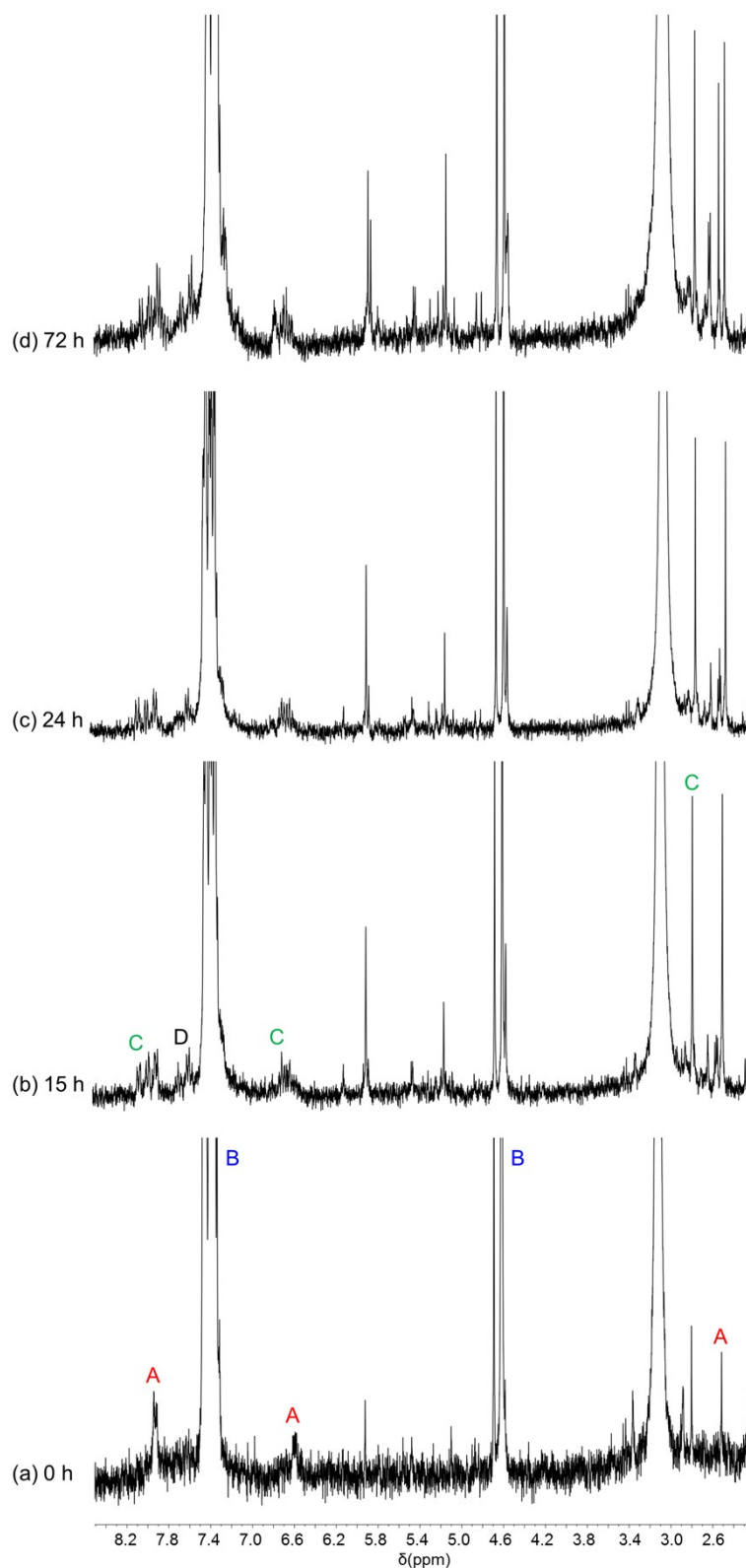


Fig. S17 The ¹H NMR spectra for the reaction of **2** with benzyl bromide in CD₃CN at different reaction times (a) 0 h, (b) 15 h, (c) 24 h, and (d) 72 h. In the spectra, A = **2**, B = benzyl bromide, C = new peaks for **3g** and D = **1**. Reaction conditions: **2** = 1.00 mg, 0.0018 mmol; benzyl bromide = 1.54 mg, 0.0090 mmol; CD₃CN = 1.00 mL; reaction temperature = 25 °C.

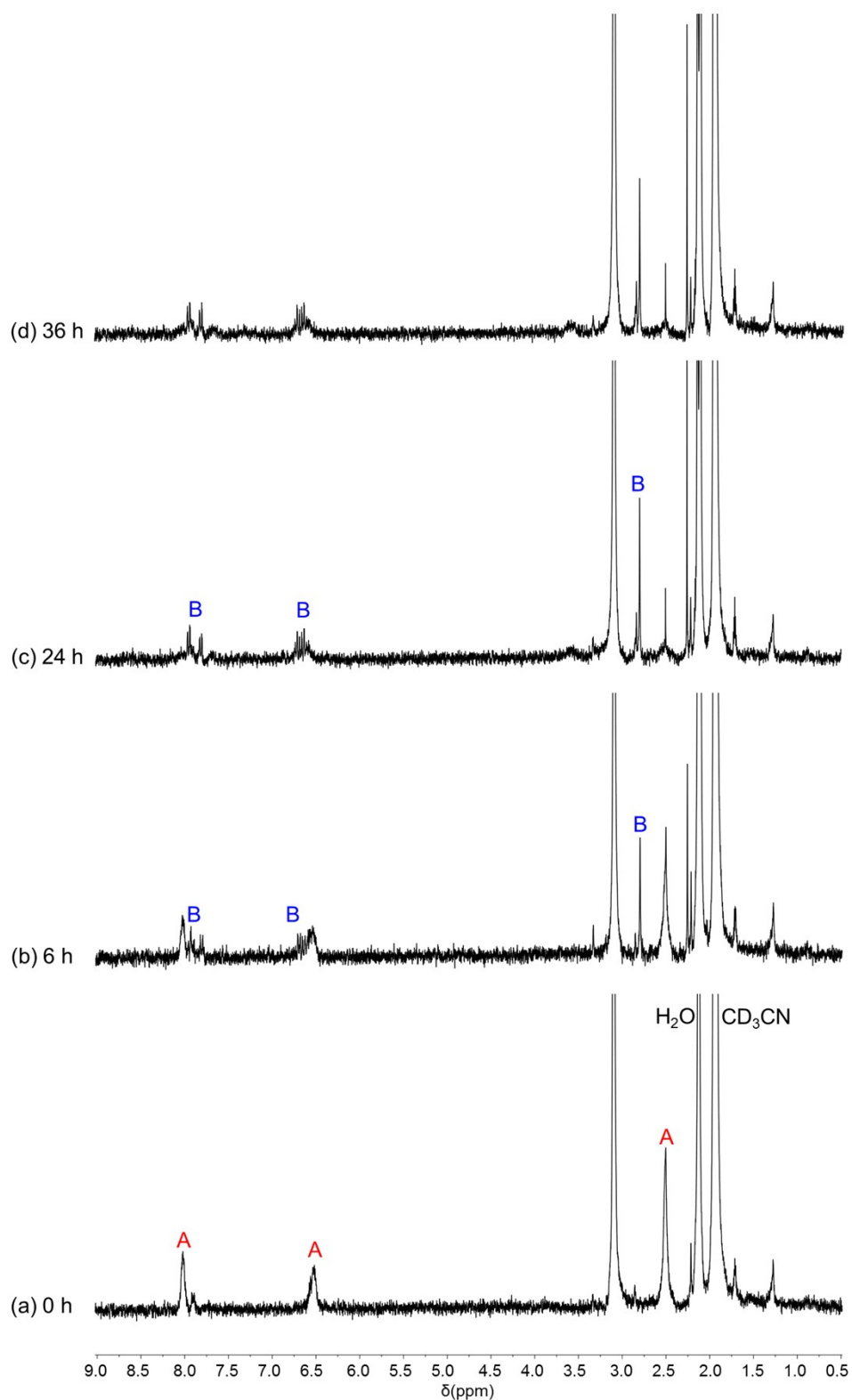


Fig. S18 The ¹H NMR spectra for the reaction of **2** with pentafluoropyridine in CD₃CN at different reaction times (a) 0 h, (b) 6 h, (c) 24 h, and (d) 36 h. In the spectra, A = **2**, and B = new peaks for product **3h**. Reaction conditions: **2** = 1.00 mg, 0.0018 mmol; pentafluoropyridine = 1.52 mg, 0.0090 mmol; CD₃CN = 1.00 mL; reaction temperature = 25 °C.

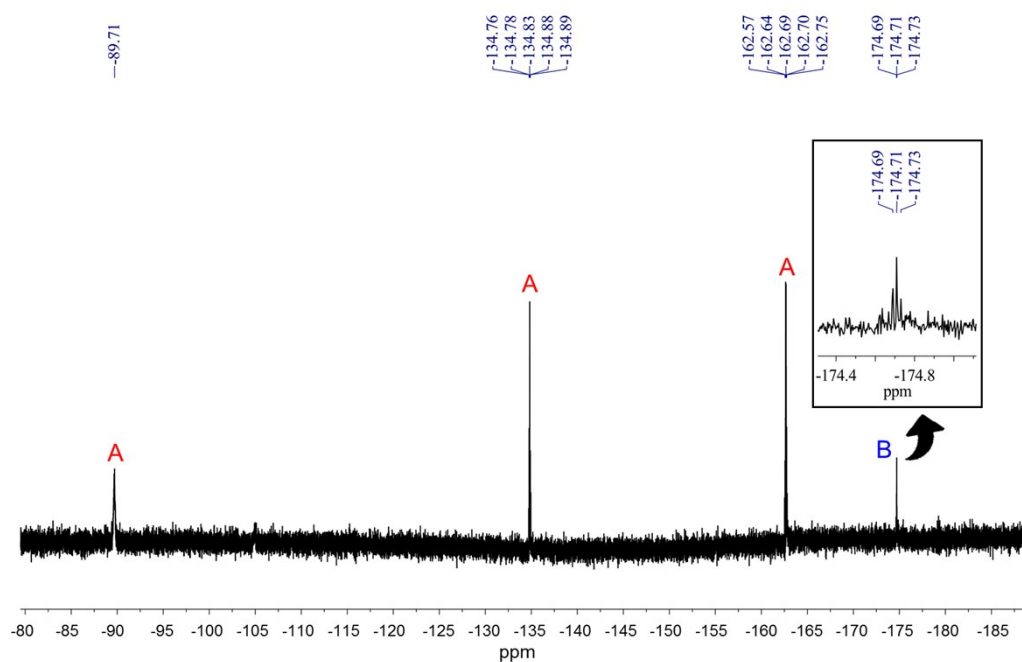


Fig. S19 The $^{19}\text{F}\{^1\text{H}\}$ NMR spectrum for the reaction of **2** with pentafluoropyridine in CD_3CN recorded after 36 h. In the spectra, A = pentafluoropyridine, and B = new peaks for product **3h**. Reaction conditions: **2** = 1.00 mg, 0.0018 mmol; pentafluoropyridine = 1.52 mg, 0.0090 mmol; CD_3CN = 1.00 mL; reaction temperature = 25 °C.

II. Electrochemistry:

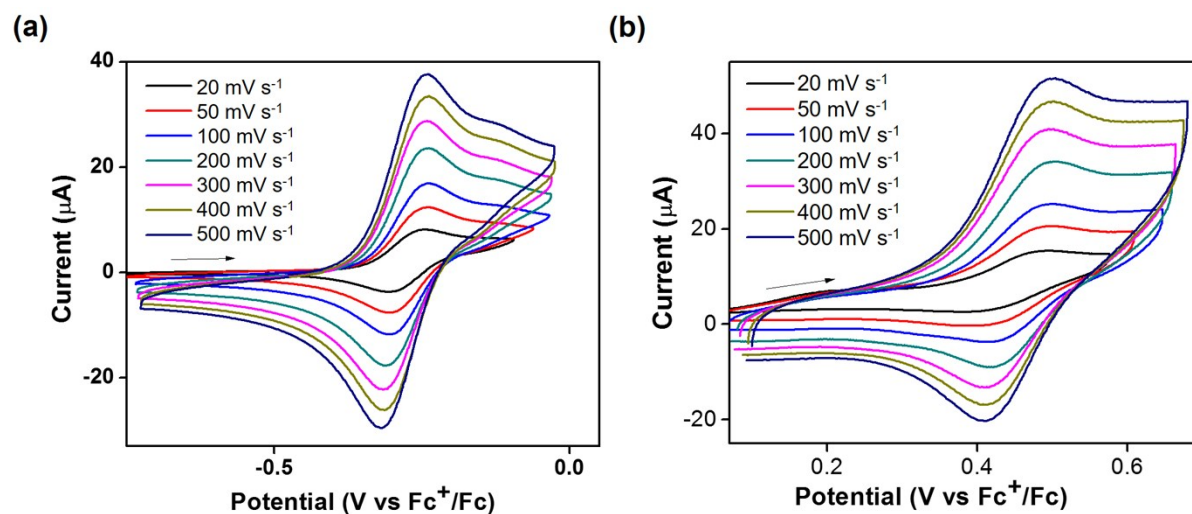


Fig. S20 Cyclic voltammograms of **2** (1.0 mM) in MeCN using $n\text{-Bu}_4\text{NPF}_6$ (0.10 M) as the electrolyte at different scan rates for (a) $\text{Ni}^{\text{III}}/\text{Ni}^{\text{II}}$ redox couple and (b) the formation of the ligand-based cation radical (glassy carbon as working electrode; two Pt wires as the auxiliary electrode and pseudo-reference electrode). The arrows indicate the directions of the scans. The former was found to be reversible, while the latter was quasi-reversible. The ligand-based cation radical formed due to the readily oxidized redox non-innocent behavior of the Me_2opba ligand.

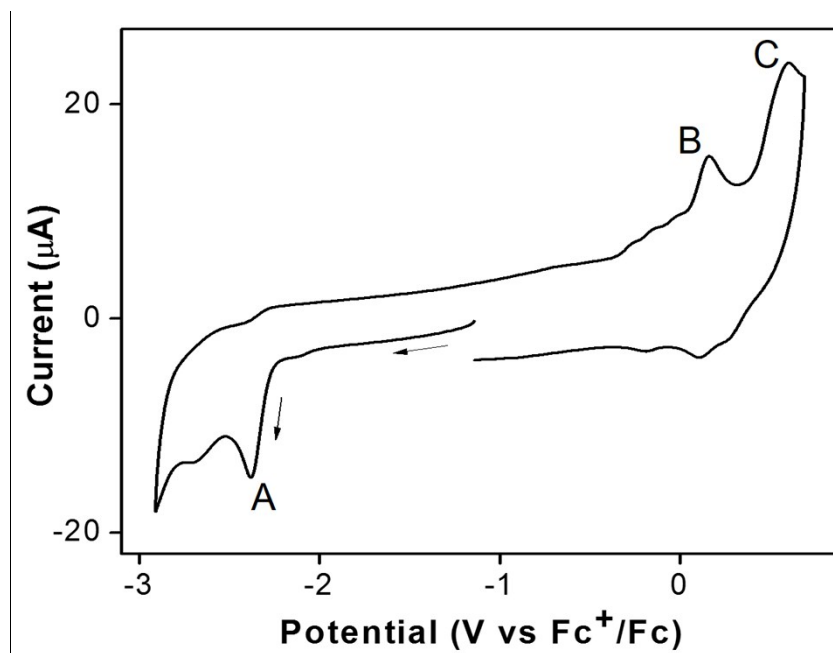


Fig. S21 Cyclic voltammogram of **3a** (1.0 mM) in DMSO using KPF₆ (0.10 M) as the supporting electrolyte under argon at a scan rate of 100 mV s⁻¹ (A, B, and C stand for the Ni^{II}/Ni^I and Ni^{III}/Ni^{II} redox couples, followed by formation of the ligand-based cation radical, respectively; glassy carbon as working electrode; two Pt wires as the auxiliary electrode and pseudo-reference electrode). The arrows indicate the directions of scans.

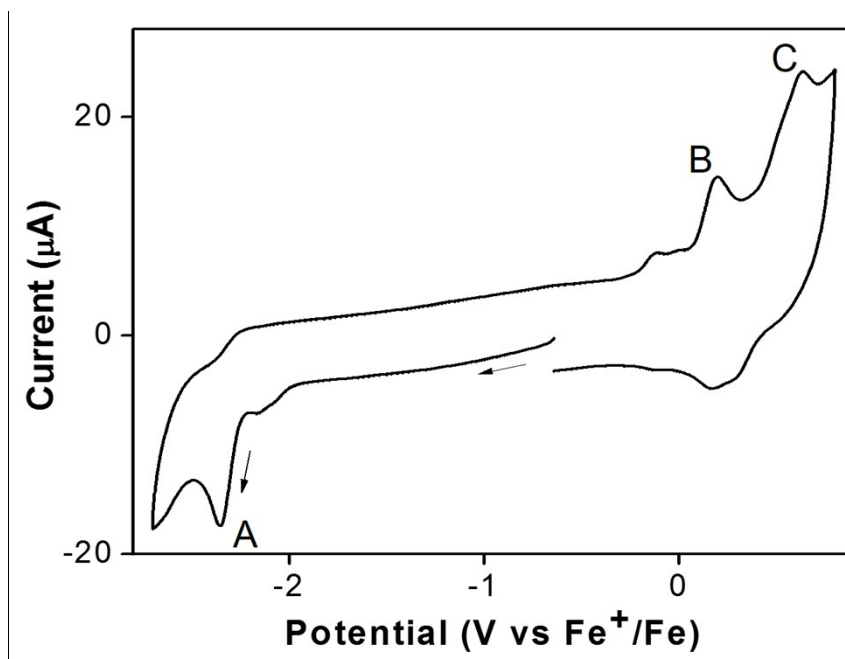


Fig. S22 Cyclic voltammogram of **3b** (1.0 mM) in DMSO using KPF₆ (0.10 M) as the supporting electrolyte under argon at a scan rate of 100 mV s⁻¹ (A, B, and C stand for the Ni^{II}/Ni^I and Ni^{III}/Ni^{II} redox couples, followed by formation of the ligand-based cation radical, respectively; glassy carbon as working electrode; two Pt wires as the auxiliary electrode and pseudo-reference electrode). The arrows indicate the directions of scans.

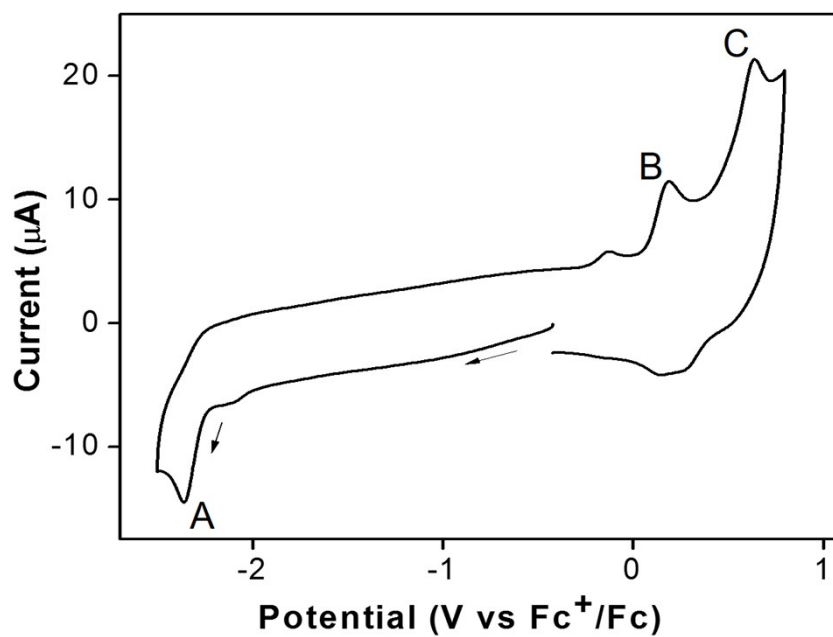


Fig. S23 Cyclic voltammogram of **3c** (1.0 mM) in DMSO using KPF₆ (0.10 M) as the supporting electrolyte under argon at a scan rate of 100 mV s⁻¹ (A, B, and C stand for the Ni^{II}/Ni^I and Ni^{III}/Ni^{II} redox couples, followed by formation of the ligand-based cation radical, respectively; glassy carbon as working electrode; two Pt wires as the auxiliary electrode and pseudo-reference electrode). The arrows indicate the directions of scans.

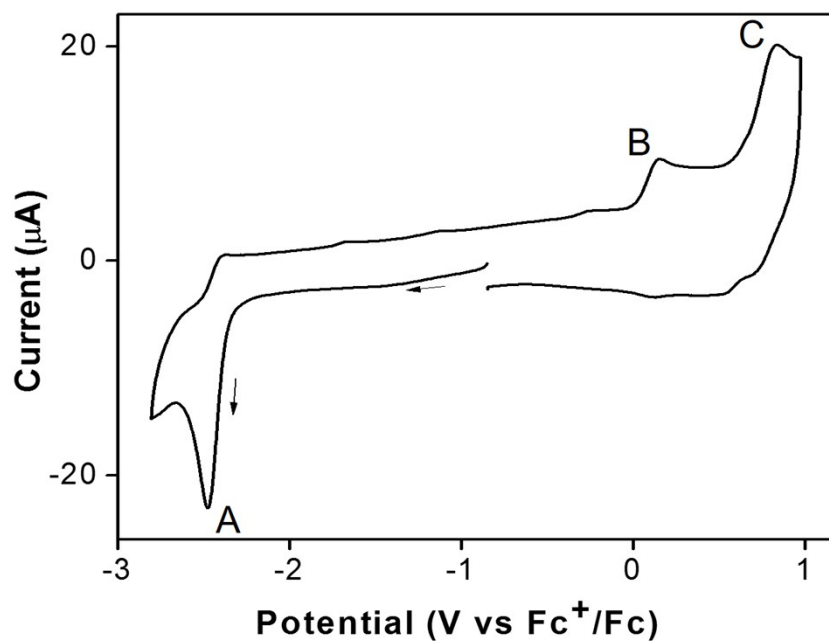


Fig. S24 Cyclic voltammogram of **3d** (1.0 mM) in MeCN using *n*-Bu₄NPF₆ (0.10 M) as the supporting electrolyte under argon at a scan rate of 100 mV s⁻¹ (A, B, and C stand for the Ni^{II}/Ni^I and Ni^{III}/Ni^{II} redox couples, followed by formation of the ligand-based cation radical, respectively; glassy carbon as working electrode; two Pt wires as the auxiliary electrode and pseudo-reference electrode). The arrows indicate the directions of scans.

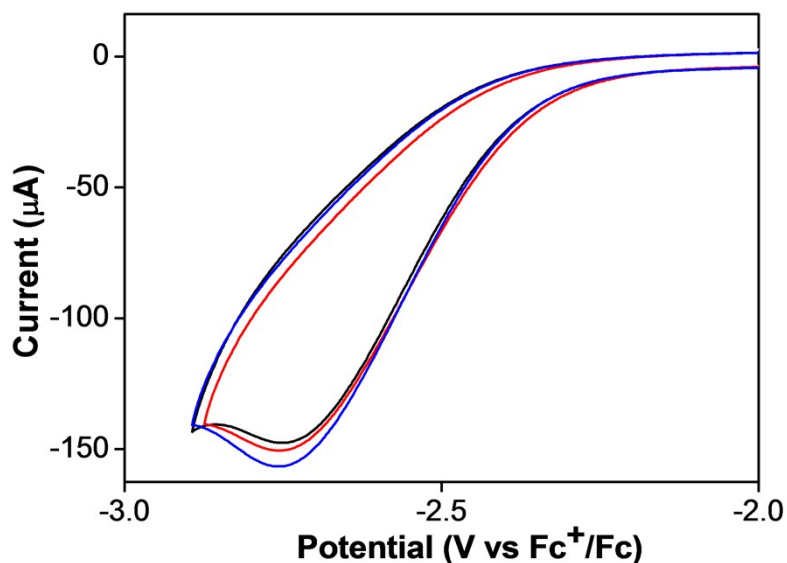


Fig. S25 Cyclic voltammograms in DMSO with KPF_6 (0.10 M) as the electrolyte under argon in the presence of 10 mM CHCl_3 only (black), 10 mM CHCl_3 (10 mM) with 20 mM *iso*-propyl alcohol (red), and 10 mM CHCl_3 with 20 mM *iso*-propyl alcohol and 1.0 mM **2** (blue) (glassy carbon as the working electrode; two Pt wires as the auxiliary electrode and pseudo-reference electrode; scan rate: 100 mV s^{-1}).

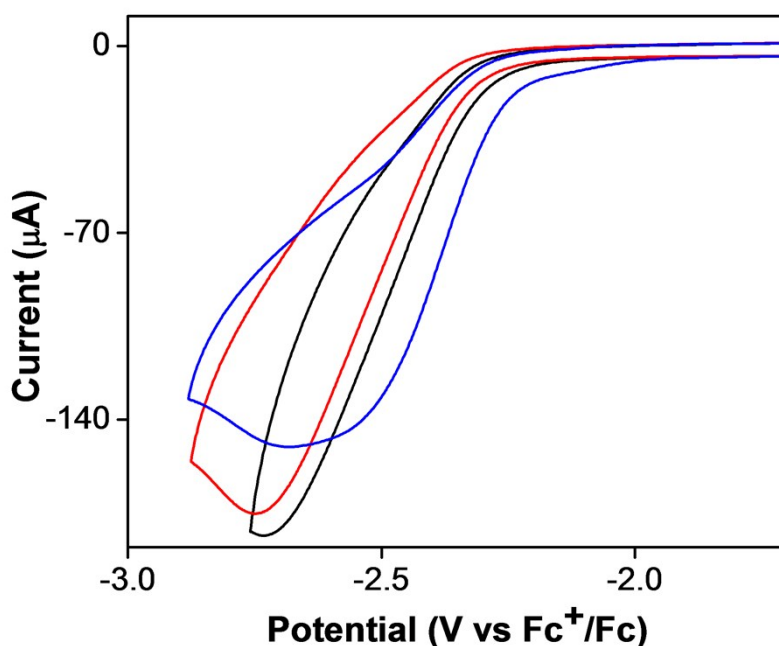


Fig. S26 Cyclic voltammograms in DMSO with KPF_6 (0.10 M) as the electrolyte under argon in the presence of 10 mM CHCl_3 only (black), 10 mM CHCl_3 (10 mM) with 20 mM *iso*-propyl alcohol (red), and 10 mM CHCl_3 with 20 mM *iso*-propyl alcohol and 1.0 mM **3a** (blue) (glassy carbon as the working electrode; two Pt wires as the auxiliary electrode and pseudo-reference electrode; scan rate: 100 mV s^{-1}).

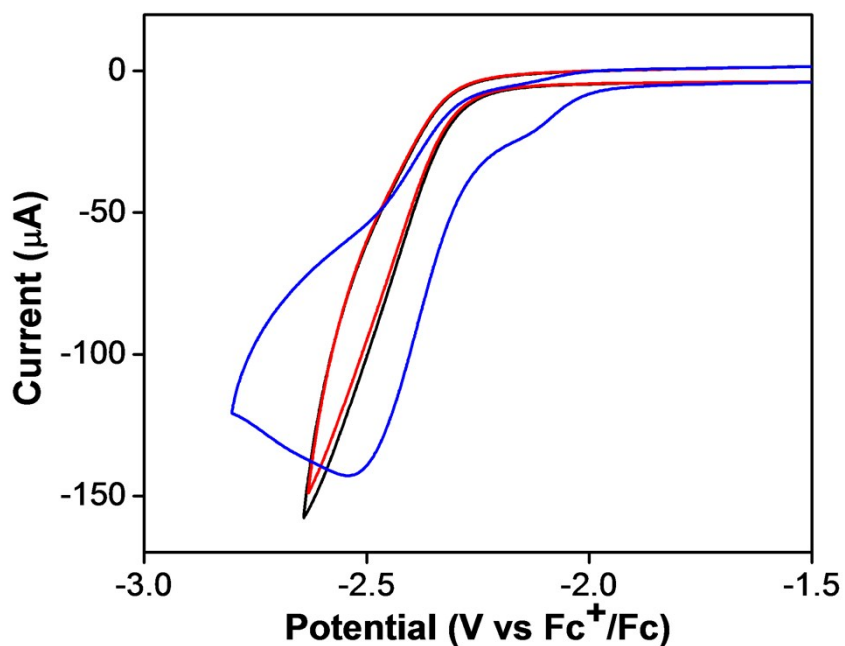


Fig. S27 Cyclic voltammograms in DMSO with KPF_6 (0.10 M) as the electrolyte under argon in the presence of 10 mM CHCl_3 only (black), 10 mM CHCl_3 (10 mM) with 20 mM *iso*-propyl alcohol (red), and 10 mM CHCl_3 with 20 mM *iso*-propyl alcohol and 1.0 mM **3b** (blue) (glassy carbon as the working electrode; two Pt wires as the auxiliary electrode and pseudo-reference electrode; scan rate: 100 mV s^{-1}).

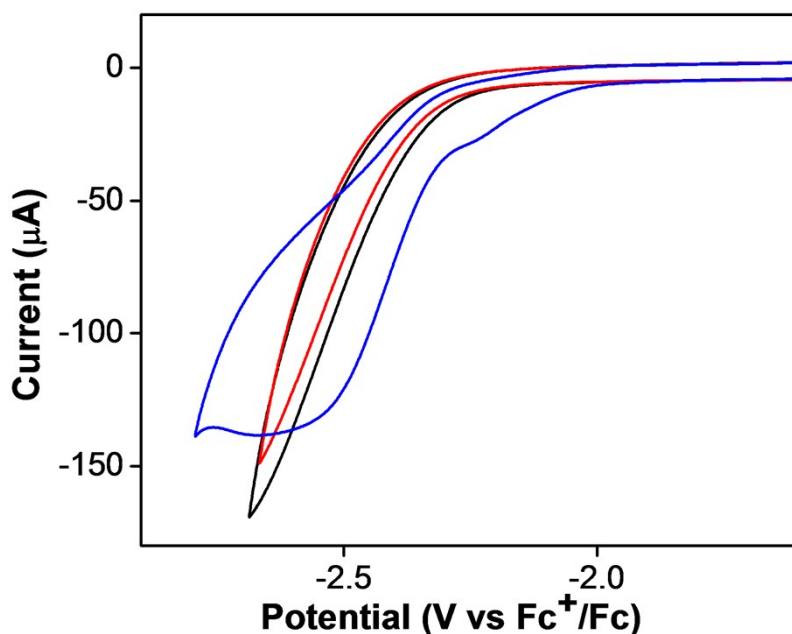


Fig. S28 Cyclic voltammograms in DMSO with KPF_6 (0.10 M) as the electrolyte under argon in the presence of 10 mM CHCl_3 only (black), 10 mM CHCl_3 (10 mM) with 20 mM *iso*-propyl alcohol (red), and 10 mM CHCl_3 with 20 mM *iso*-propyl alcohol and 1.0 mM **3c** (blue) (glassy carbon as the working electrode; two Pt wires as the auxiliary electrode and pseudo-reference electrode; scan rate: 100 mV s^{-1}).

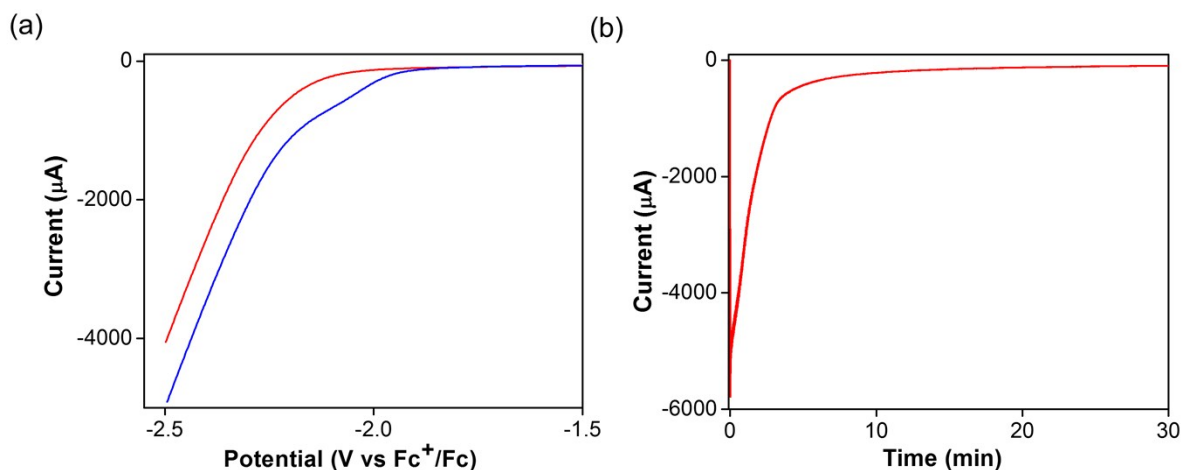


Fig. S29 Electrochemical CHCl_3 reduction activity with complex **3b**. (a) Traces for linear sweep voltammetry (LSV) experiment in the absence (red) or presence of 1.0 mM **3b** (blue) in DMSO with 0.10 M KPF_6 as the electrolyte, 50 mM CHCl_3 , and 100 mM *iso*-propyl alcohol under argon. (b) CPE for the reduction of CHCl_3 in DMSO (15 mL) at -2.5 V for 30 min in the presence of **3b** (1.0 mM) (0.10 M KPF_6 , 50 mM benzene, 50 mM CHCl_3 , and 100 mM *iso*-propyl alcohol under argon).

Analytical measurements to detect heterogeneous electrocatalysis

We attempted to identify the inactive catalyst by-products after the electrolysis with ^1H NMR spectroscopy. Upon removal of the DMSO under reduced pressure, the ^1H NMR spectrum showed only the uncoordinated ligand **1**, suggesting that **2** had hydrolyzed. Moreover, transmission electron microscopy (TEM) and dynamic light scattering (DLS) experiments on the spent electrolysis solution did not show nanoparticles in the reaction mixture. Instead, the TEM images showed micron-sized crystalline chunks that concurred with DLS measurements (particles > 1000 nm), and the microcrystals likely arose from the copious amounts of precipitated KPF_6 electrolyte (Fig. S35, ESI).

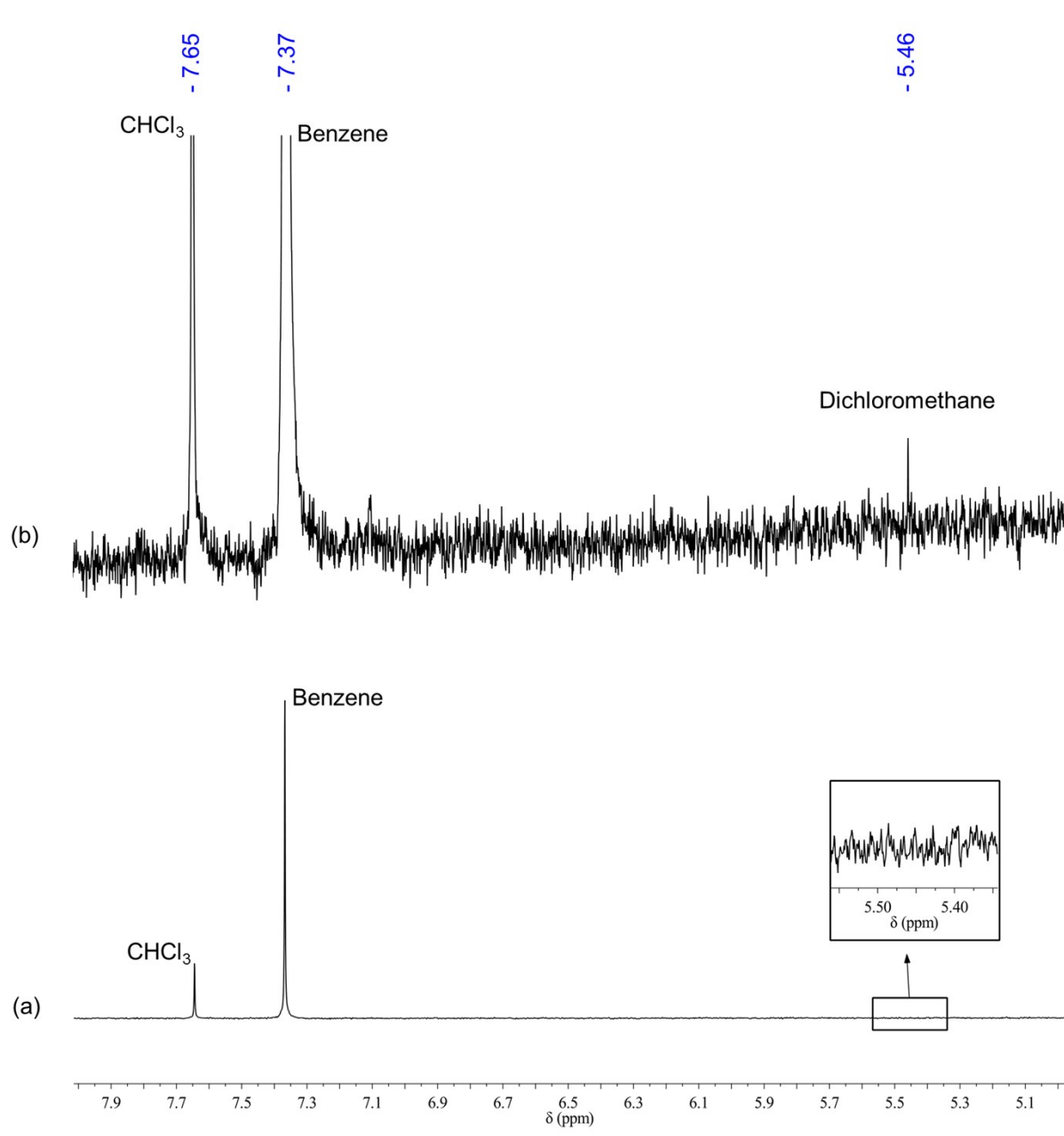


Fig. S30 The ^1H NMR spectra in CD_3CN of an aliquot of a reaction mixture (a) before and (b) after a 30 min CPE experiment at -2.50 V (vs Fc^+/Fc). The reaction mixture contained DMSO (15 mL), KPF_6 (0.10 M), benzene (50 mM), CHCl_3 (50 mM), *iso*-propyl alcohol (100 mM), and **3d** (1.0 mM). The spectrum (b) shows the presence of dichloromethane (5.46 ppm) in the reaction mixture after CPE.

Calculations to determine the % conversion of CHCl₃ and the turnover numbers (TON) from the ¹H NMR spectra

The % conversions of CHCl₃ in the CPE experiments were calculated on the basis of the integrated area of the CHCl₃ peak ($\delta = \sim 7.65$ ppm). In each reaction, benzene (50 mM) was added as an internal standard for the ¹H NMR spectroscopic measurements. A representative calculation for the % conversion of CHCl₃ catalyzed by **3d** is shown here:

Integrated area before CPE = 0.99 (corresponds to 50 mM of CHCl₃)

Integrated area after CPE = 0.88

Therefore, CHCl₃ concentration in the reaction mixture after CPE = $(0.88 * 50 / 0.99)$ mM
= 44.4 mM

Amount of CHCl₃ reacted = $50.0 - 44.4 = 5.6$ mM

% CHCl₃ conversion = $5.6 * 100 / 50 = 11\%$

Since the concentration of **3d** in the reaction mixture = 1.0 mM

Therefore, TON = $5.6 / 1.0 = 5.6$

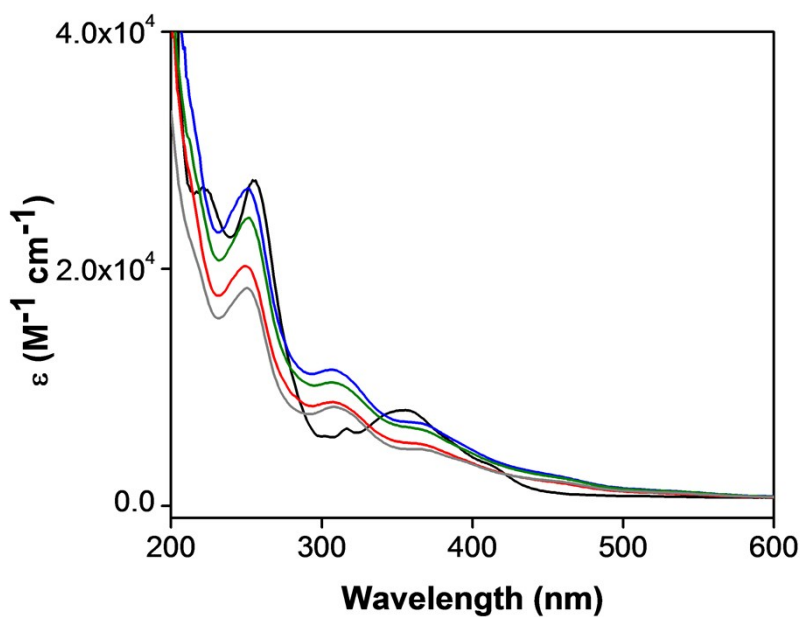


Fig. S31 UV-visible spectra for complexes **2** (black), **3a** (red), **3b** (blue), **3c** (green), and **3d** (grey) in 0.10 mM MeCN.

Table S1 UV-visible spectral data for complexes **2** and **3** in MeCN.

Complex	λ_{max} (nm)	ϵ ($\text{M}^{-1} \text{cm}^{-1}$)
2	255	357
	(27600)	(8090)
3a	250	361 (sh)
	(20300)	(8770)
3b	251	361 (sh)
	(26900)	(11500)
3c	252	359 (sh)
	(24400)	(10400)
3d	251	362 (sh)
	(18400)	(8390)

sh = shoulder

Characterization of the halide by-product after reaction between **2** and alkyl halide

The characterization of the halide by-product after the reaction between **2** and the alkyl halides was conducted by using methyl iodide as a representative substrate. In a typical procedure, after the extraction of **3a** from the reaction mixture as detailed in the Experimental Section of the main manuscript, the residue was washed thrice with hexane. Subsequently, the remaining solid was dried under reduced pressure. The ^1H NMR spectrum in CD_3CN and the ESI-MS in MeOH of the dried residue are shown in Figures S32 – S34. The ^1H NMR spectrum shows a singlet at $\delta = 3.09$ ppm, which corresponds to the Me_4N^+ cation. Apart from this, there are no additional peaks in the spectrum in the range of $\delta = -1$ to 22 ppm. This suggests that the Me_4N^+ cation is the main organic component in this residue, which has been verified by the ESI-MS in the positive ion mode, which displays a signal at $m/z = 74.22$ Da (Fig. S34), which matches the molecular weight of the Me_4N^+ cation. The ESI-MS in the negative ion model shows a prominent peak at $m/z = 126.83$ (Fig. S33), which corresponds to I^- . These observations strongly indicate that the predominant by-product present in the solid residue is Me_4NI .

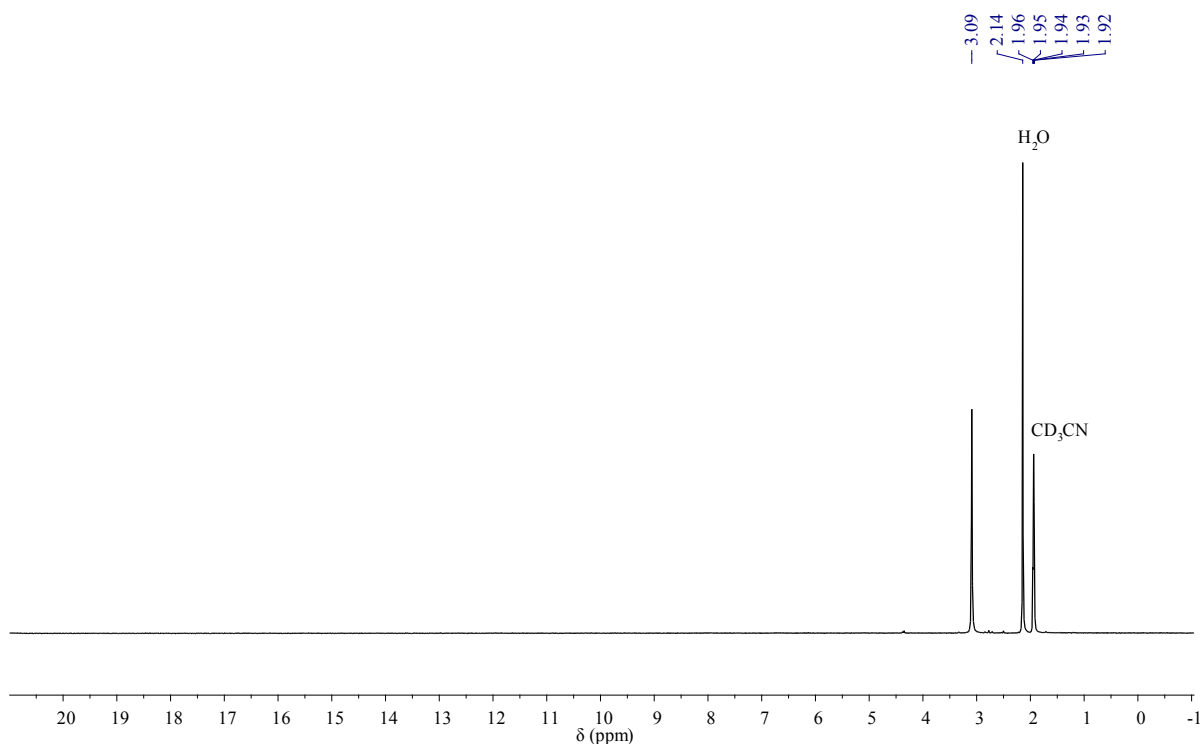


Fig. S32 The ¹H NMR spectrum of the solid residue recorded in CD₃CN from the reaction mixture between **2** and methyl iodide, after removal of **3a**. The peak at 3.09 ppm likely corresponds to the NMe₄⁺ cation.

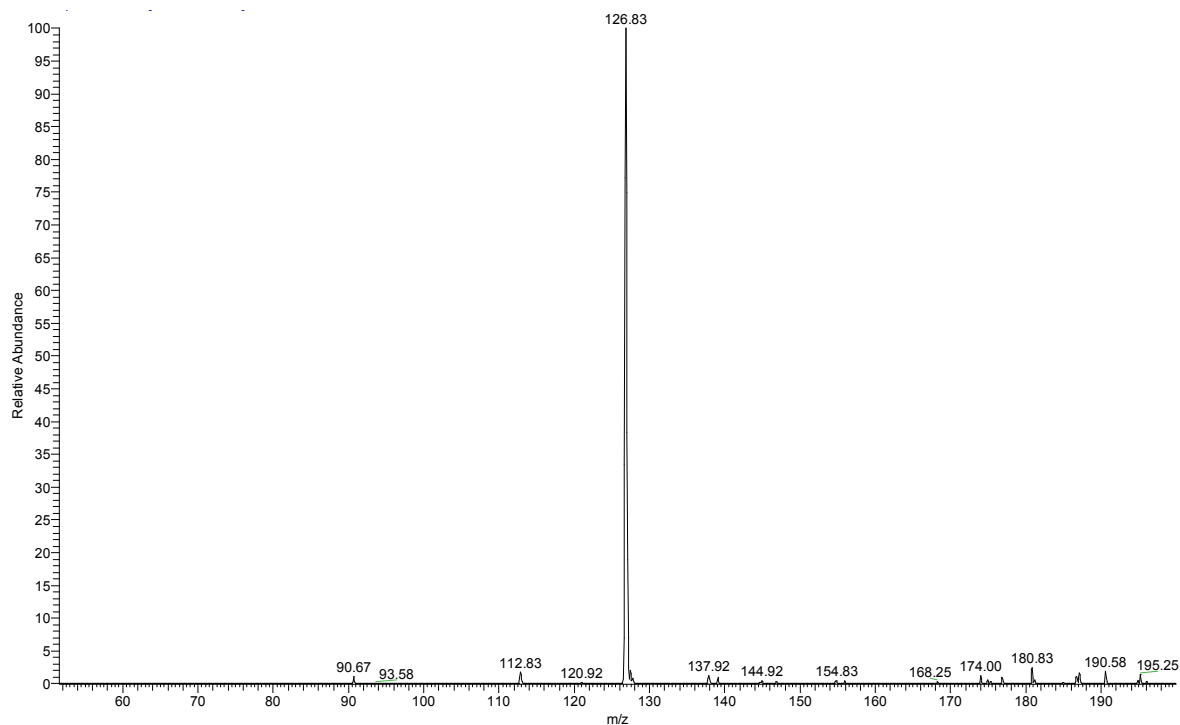


Fig. S33 ESI-MS of the solid residue recorded in MeOH from the reaction mixture between **2** and methyl iodide, after removal of **3a**, showing a signal at $m/z = 126.83$ Da for I⁻.

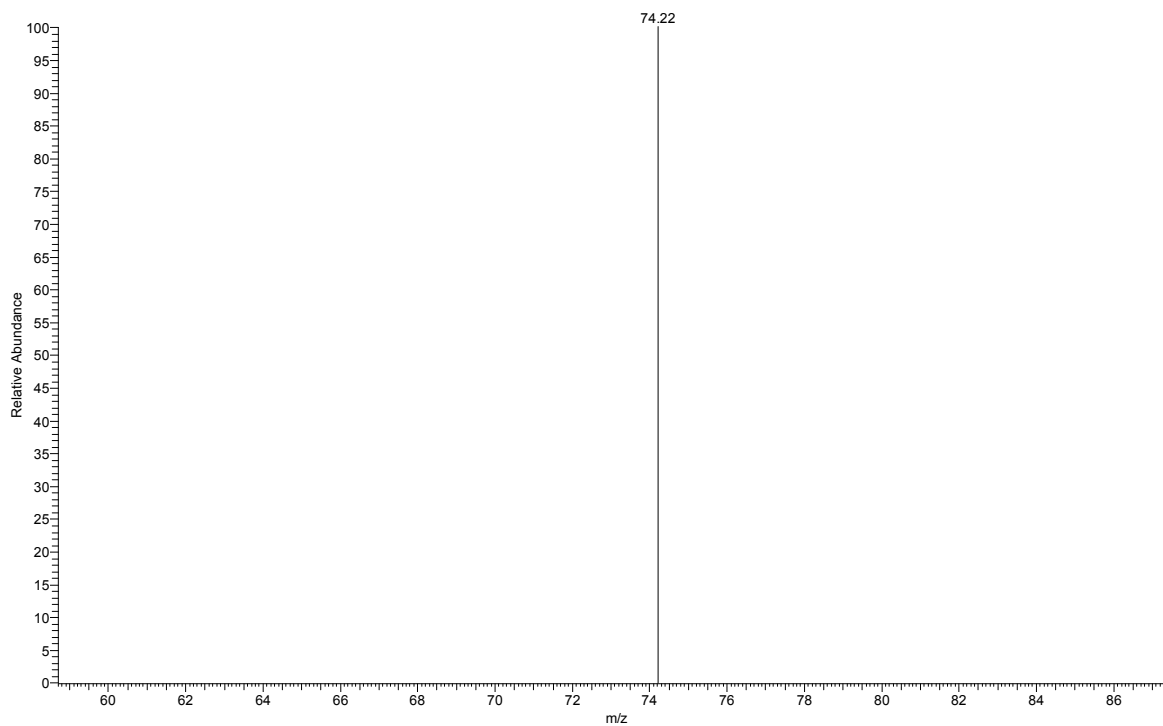


Fig. S34 ESI-MS of the solid residue recorded in MeOH from the reaction mixture between **2** and methyl iodide, after removal of **3a**, showing a signal at $m/z = 74.22$ Da for Me_4N^+ .

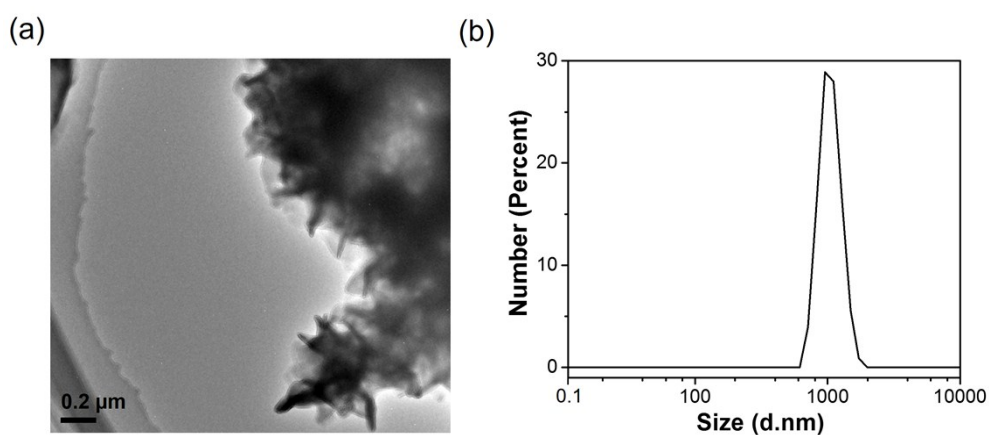


Fig. S35 (a) TEM image and (b) DLS profile of the reaction mixture after a 30 min CPE experiment. The reaction mixture contained DMSO (15 mL), KPF_6 (0.10 M), benzene (50 mM), CHCl_3 (50 mM), *iso*-propyl alcohol (100 mM), and **2** (1.0 mM). The DLS measurement was done with the spent reaction mixture at 20 °C. The TEM image was recorded after removing the DMSO under reduced pressure from the spent reaction mixture. The data indicate the presence of microcrystalline materials that are likely to be the precipitated KPF_6 electrolyte.

III. X-Ray Crystallography

(i) Complex 3a

A red plate-like specimen of **3a**, with approximate dimensions 0.020 mm x 0.100 mm x 0.160 mm, was used for the X-ray crystallographic analysis. The X-ray intensity data were measured with a Bruker Kappa diffractometer equipped with a CCD detector, employing Mo K α radiation ($\lambda = 0.71073 \text{ \AA}$), with the SMART suite of programs.² The total exposure time was 3.25 hours. The frames were integrated with the Bruker SAINT software package using a narrow-frame algorithm. The integration of the data using a monoclinic unit cell yielded a total of 16450 reflections to a maximum θ angle of 26.39° (0.80 \AA resolution), of which 3920 were independent (average redundancy = 4.196, completeness = 99.7%, $R_{\text{int}} = 13.13\%$, $R_{\text{sig}} = 14.80\%$) and 2041 (52.07%) were greater than $2\sigma(F^2)$. The final cell constants of $\underline{a} = 29.263(2) \text{ \AA}$, $\underline{b} = 12.4118(9) \text{ \AA}$, $\underline{c} = 10.6811(9) \text{ \AA}$, $\beta = 99.098(3)^\circ$, volume = $3830.6(5) \text{ \AA}^3$, are based upon the refinement of the XYZ-centroids of 2046 reflections above $20 \sigma(I)$ with $5.094^\circ < 2\theta < 51.75^\circ$. Data were corrected for absorption effects using the multi-scan method (SADABS).³ Structural solution and refinement were carried out with the SHELXTL suite of programs.⁴ The ratio of minimum to maximum apparent transmission was 0.761. The calculated minimum and maximum transmission coefficients (based on crystal size) are 0.8500 and 0.9790. The final anisotropic full-matrix least-squares refinement on F^2 with 251 variables converged at $R1 = 6.22\%$ for the observed data, and $wR2 = 17.21\%$ for all data. The goodness-of-fit was 1.100. The largest peak in the final difference electron density synthesis was $0.600 \text{ e}/\text{\AA}^3$ and the largest hole was $-0.809 \text{ e}/\text{\AA}^3$ with a RMS deviation of $0.123 \text{ e}/\text{\AA}^3$. On the basis of the final model, the calculated density was $1.464 \text{ g}/\text{cm}^3$ and $F(000)$ was 1776 e.

(ii) Complex 3b

A red plate-like specimen of **3b**, with approximate dimensions 0.020 mm x 0.200 mm x 0.400 mm, was used for the X-ray crystallographic analysis. The X-ray intensity data were measured with a Bruker Kappa diffractometer equipped with a CCD detector, employing Mo K α radiation ($\lambda = 0.71073 \text{ \AA}$), with the SMART suite of programs.² The total exposure time was 1.48 hours. The frames were integrated with the Bruker SAINT software package using a narrow-frame algorithm. The integration of the data using a monoclinic unit cell yielded a total of 24374 reflections to a maximum θ angle of 30.07° (0.71 \AA resolution), of which 5732 were independent (average redundancy = 4.252, completeness = 99.7%, $R_{\text{int}} = 12.48\%$, $R_{\text{sig}} = 15.26\%$) and 2854 (49.79%) were greater than $2\sigma(F^2)$. The final cell constants of $a = 25.970(3) \text{ \AA}$, $b = 8.6558(7) \text{ \AA}$, $c = 18.0823(17) \text{ \AA}$, $\beta = 105.855(3)^\circ$, volume = $3910.1(6) \text{ \AA}^3$, are based upon the refinement of the XYZ-centroids of 3630 reflections above $20 \sigma(I)$ with $4.683^\circ < 2\theta < 48.47^\circ$. Data were corrected for absorption effects using the Multi-Scan method (SADABS).³ The ratio of minimum to maximum apparent transmission was 0.827. The calculated minimum and maximum transmission coefficients (based on crystal size) are 0.6840 and 0.9800. The structure was solved and refined using the Bruker SHELXTL Software Package,⁶ using the space group $C 1 2/c 1$, with $Z = 8$ for the formula unit, $C_{18}H_{27}N_5NiO_4$. The final anisotropic full-matrix least-squares refinement on F^2 with 260 variables converged at $R1 = 6.68\%$ for the observed data, and $wR2 = 16.88\%$ for all data. The goodness-of-fit was 0.988. The largest peak in the final difference electron density synthesis was $1.469 \text{ e}/\text{\AA}^3$ and the largest hole was $-0.516 \text{ e}/\text{\AA}^3$ with a RMS deviation of $0.121 \text{ e}/\text{\AA}^3$. On the basis of the final model, the calculated density was 1.482 g/cm^3 and $F(000)$ was 1840 e.

(iii) Complex 3c

A red plate-like specimen of **3c**, with approximate dimensions 0.005 mm x 0.100 mm x 0.140 mm, was used for the X-ray crystallographic analysis. The X-ray intensity data were measured with a Bruker Kappa diffractometer equipped with a CCD detector, employing Cu K α -microfocus radiation ($\lambda = 1.54178 \text{ \AA}$), with the SMART suite of programs.² The total exposure time was 10.34 hours. The frames were integrated with the Bruker SAINT software package using a narrow-frame algorithm. The integration of the data using a monoclinic unit cell yielded a total of 7340 reflections to a maximum θ angle of 66.65° (0.84 \AA resolution), of which 7340 were independent (average redundancy = 5.09, completeness = 99.1%, $R_{\text{sig}} = 3.75\%$) and 6483 (88.32%) were greater than $2\sigma(F^2)$. The final cell constants of $\underline{a} = 15.8813(4) \text{ \AA}$, $\underline{b} = 24.8528(6) \text{ \AA}$, $\underline{c} = 10.6517(3) \text{ \AA}$, $\beta = 94.7164(15)^\circ$, volume = $4189.93(19) \text{ \AA}^3$, are based upon the refinement of the XYZ-centroids of 9849 reflections above $20 \sigma(I)$ with $7.113^\circ < 2\theta < 132.7^\circ$. Data were corrected for absorption effects using the Multi-Scan method (SADABS).³ The crystals of **3c** were found to be twinned; the twin law and cell parameters were determined using the program CELL_NOW,⁵ and the reflection data were processed and corrections applied using the program TWINABS.⁶ Structural solution and refinement were carried out with the SHELXTL suite of programs.⁴ The ratio of minimum to maximum apparent transmission was 0.614. The calculated minimum and maximum transmission coefficients (based on crystal size) are 0.8030 and 0.9920. The final anisotropic full-matrix least-squares refinement on F^2 with 539 variables converged at $R1 = 4.59\%$ for the observed data, and $wR2 = 12.39\%$ for all data. The goodness-of-fit was 1.087. The largest peak in the final difference electron density synthesis was $0.403 \text{ e}^-/\text{\AA}^3$ and the largest hole was $-0.413 \text{ e}^-/\text{\AA}^3$ with a RMS deviation of $0.062 \text{ e}^-/\text{\AA}^3$. On the basis of the final model, the calculated density was 1.427 g/cm^3 and $F(000)$ was 1904 e^- .

(iv) Complex 3d

A red plate-like specimen of **3d**, with approximate dimensions 0.040 mm x 0.320 mm x 0.420 mm, was used for the X-ray crystallographic analysis. The X-ray intensity data were measured with a Bruker Kappa diffractometer equipped with a CCD detector, employing Mo K_{α} radiation ($\lambda = 0.71073 \text{ \AA}$), with the SMART suite of programs.² The total exposure time was 2.12 hours. The frames were integrated with the Bruker SAINT software package using a narrow-frame algorithm. The integration of the data using a monoclinic unit cell yielded a total of 43588 reflections to a maximum θ angle of 31.12° (0.69 \AA resolution), of which 7173 were independent (average redundancy = 6.077, completeness = 99.6%, $R_{\text{int}} = 8.51\%$, $R_{\text{sig}} = 6.97\%$) and 4017 (56.00%) were greater than $2\sigma(F^2)$. The final cell constants of $\underline{a} = 19.1442(14) \text{ \AA}$, $\underline{b} = 10.1337(7) \text{ \AA}$, $\underline{c} = 11.8238(8) \text{ \AA}$, $\beta = 102.976(2)^{\circ}$, volume = $2235.3(3) \text{ \AA}^3$, are based upon the refinement of the XYZ-centroids of 5305 reflections above $20 \sigma(I)$ with $4.366^{\circ} < 2\theta < 45.82^{\circ}$. Data were corrected for absorption effects using the Multi-Scan method (SADABS).³ The ratio of minimum to maximum apparent transmission was 0.823. The calculated minimum and maximum transmission coefficients (based on crystal size) are 0.7030 and 0.9650. The structure was solved and refined using the Bruker SHELXTL Software Package,⁴ using the space group P 1 21/c 1, with $Z = 4$ for the formula unit, $\text{C}_{20}\text{H}_{31}\text{N}_5\text{NiO}_4$. The final anisotropic full-matrix least-squares refinement on F^2 with 327 variables converged at $R1 = 5.29\%$ for the observed data, and $wR2 = 15.19\%$ for all data. The goodness-of-fit was 1.010. The largest peak in the final difference electron density synthesis was $0.507 \text{ e}/\text{\AA}^3$ and the largest hole was $-0.554 \text{ e}/\text{\AA}^3$ with a RMS deviation of $0.076 \text{ e}/\text{\AA}^3$. On the basis of the final model, the calculated density was 1.379 g/cm^3 and $F(000)$ was 984 e.

X-ray crystallographic coordinates for structures

Complexes **3a-d** reported herein have been deposited at the Cambridge Crystallographic Data Centre (CCDC), under deposition numbers CCDC 1475486-1475489. These data can be obtained free of charge from the Cambridge Crystallographic Data Centre via www.ccdc.cam.ac.uk/data_request/cif.

Table S2 Crystal data and structure refinement for complex **3a**.

Chemical formula	C ₁₇ H ₂₅ N ₅ NiO ₄
Formula weight	422.13 g/mol
Temperature	153(2) K
Wavelength	0.71073 Å
Crystal size	0.020 x 0.100 x 0.160 mm
Crystal habit	red plate
Crystal system	monoclinic
Space group	C 1 2/c 1
Unit cell dimensions	a = 29.263(2) Å α = 90° b = 12.4118(9) Å β = 99.098(3)° c = 10.6811(9) Å γ = 90°
Volume	3830.6(5) Å ³
Z	8
Density (calculated)	1.464 g/cm ³
Absorption coefficient	1.046 mm ⁻¹
F(000)	1776
Theta range for data collection	1.79 to 26.39°
Index ranges	-36 ≤ h ≤ 36, -15 ≤ k ≤ 15, -8 ≤ l ≤ 13
Reflections collected	16450
Independent reflections	3920 [R(int) = 0.1313]
Coverage of independent reflections	99.7%
Absorption correction	multi-scan
Max. and min. transmission	0.9790 and 0.8500
Refinement method	Full-matrix least-squares on F ²
Refinement program	SHELXL-2014/7 (Sheldrick, 2014)
Function minimized	Σ w(F _o ² - F _c ²) ²
Data / restraints / parameters	3920 / 0 / 251
Goodness-of-fit on F²	1.100
Final R indices	2041 data; R1 = 0.0622, wR2 = 0.1237 I > 2σ(I) all data R1 = 0.1566, wR2 = 0.1721
Weighting scheme	w = 1/[σ ² (F _o ²) + (0.0579P) ² + 3.5732P] where P = (F _o ² + 2F _c ²)/3
Largest diff. peak and hole	0.600 and -0.809 eÅ ⁻³
R.M.S. deviation from mean	0.123 eÅ ⁻³

Table S3 Selected bond lengths (Å) for complex **3a**.

Ni1-N2	1.838(5)	Ni1-N1	1.844(5)
Ni1-N4	1.894(5)	Ni1-N3	1.929(5)
C7-O2	1.234(7)	C7-N2	1.337(8)
C7-C8	1.530(8)	C8-N3	1.288(7)
C8-O3	1.330(7)	C9-O1	1.238(7)
C9-N1	1.348(7)	C9-C10	1.535(8)
C10-O4	1.245(7)	C10-N4	1.330(7)
C11-O3	1.455(7)		

Table S4 Selected bond angles (°) for complex **3a**.

N2-Ni1-N1	83.9(2)	N2-Ni1-N4	168.9(2)
N1-Ni1-N4	85.1(2)	N2-Ni1-N3	83.7(2)
N1-Ni1-N3	167.5(2)	N4-Ni1-N3	107.3(2)
C2-C1-N1	127.7(5)	C5-C6-N2	128.2(6)
N1-C1-C6	112.2(5)	N2-C6-C1	111.6(5)
O2-C7-N2	129.5(6)	O2-C7-C8	122.2(6)
N2-C7-C8	108.3(6)	N3-C8-O3	119.2(6)
N3-C8-C7	115.8(6)	O3-C8-C7	125.0(6)
O1-C9-N1	128.7(5)	O1-C9-C10	121.0(6)
N1-C9-C10	110.3(5)	O4-C10-N4	127.7(6)
O4-C10-C9	119.2(6)	N4-C10-C9	113.1(5)
C9-N1-C1	127.0(5)	C9-N1-Ni1	116.7(4)
C1-N1-Ni1	115.9(4)	C7-N2-C6	124.8(5)
C7-N2-Ni1	118.7(4)	C6-N2-Ni1	116.3(4)
C8-N3-C12	116.6(5)	C8-N3-Ni1	113.2(4)
C12-N3-Ni1	130.1(4)	C10-N4-C13	116.8(5)
C10-N4-Ni1	113.9(4)	C13-N4-Ni1	129.2(4)
C8-O3-C11	122.1(5)		

Table S5 Atomic coordinates and equivalent isotropic atomic displacement parameters (\AA^2) for complex **3a**.

U(eq) is defined as one third of the trace of the orthogonalized U_{ij} tensor.

	x/a	y/b	z/c	U(eq)
Ni1	0.67579(2)	0.81458(6)	0.45166(7)	0.0306(3)
C1	0.6098(2)	0.6640(4)	0.3567(5)	0.0302(14)
C2	0.5710(2)	0.5993(4)	0.3352(6)	0.0374(15)
C3	0.5674(2)	0.5251(5)	0.2366(6)	0.0458(18)
C4	0.6018(2)	0.5162(5)	0.1622(6)	0.0474(18)
C5	0.6397(2)	0.5810(5)	0.1819(6)	0.0421(16)
C6	0.6442(2)	0.6552(4)	0.2783(5)	0.0309(14)
C7	0.7156(2)	0.7457(5)	0.2498(6)	0.0400(16)
C8	0.7473(2)	0.8316(5)	0.3199(6)	0.0352(15)
C9	0.5924(2)	0.7811(4)	0.5294(5)	0.0339(15)
C10	0.6159(2)	0.8742(5)	0.6095(5)	0.0342(15)
C11	0.8061(2)	0.8192(5)	0.1821(7)	0.0545(19)
C12	0.7653(2)	0.9558(5)	0.4911(6)	0.0514(19)
C13	0.6862(2)	0.9732(5)	0.6733(6)	0.0505(18)
C14	0.5498(2)	0.8084(5)	0.0988(5)	0.0438(16)
C15	0.5358(2)	0.9215(5)	0.9099(6)	0.0389(16)
C16	0.5519(2)	0.7296(5)	0.8901(6)	0.0459(17)
C17	0.61349(19)	0.8490(5)	0.9827(6)	0.0420(16)
N1	0.62024(16)	0.7440(3)	0.4497(4)	0.0290(11)
N2	0.68056(17)	0.7287(4)	0.3141(4)	0.0339(12)
N3	0.73433(15)	0.8710(4)	0.4202(5)	0.0327(12)
N4	0.65908(17)	0.8921(4)	0.5903(4)	0.0339(12)
N5	0.56267(15)	0.8270(4)	0.9704(4)	0.0318(12)
O1	0.55333(14)	0.7496(3)	0.5427(4)	0.0445(11)
O2	0.72332(15)	0.7042(4)	0.1504(5)	0.0565(13)
O3	0.78506(14)	0.8708(3)	0.2814(4)	0.0477(12)
O4	0.59397(15)	0.9232(3)	0.6825(4)	0.0480(12)

Table S6 Anisotropic atomic displacement parameters (\AA^2) for complex **3a**.

The anisotropic atomic displacement factor exponent takes the form:

$$-2\pi^2 [h^2 a^{*2} U_{11} + \dots + 2 h k a^* b^* U_{12}]$$

	U_{11}	U_{22}	U_{33}	U_{23}	U_{13}	U_{12}
Ni1	0.0331(5)	0.0275(4)	0.0312(4)	0.0029(4)	0.0052(3)	0.0020(4)
C1	0.040(4)	0.022(3)	0.027(3)	0.000(3)	-0.001(3)	0.000(3)
C2	0.047(4)	0.031(3)	0.033(3)	0.007(3)	0.001(3)	-0.002(3)
C3	0.053(5)	0.030(4)	0.048(4)	0.002(3)	-0.010(4)	-0.009(3)
C4	0.069(5)	0.035(4)	0.038(4)	-0.008(3)	0.006(4)	0.008(4)
C5	0.045(4)	0.038(4)	0.044(4)	-0.009(3)	0.010(3)	0.002(3)
C6	0.037(4)	0.030(3)	0.027(3)	0.001(3)	0.007(3)	0.008(3)
C7	0.045(4)	0.029(4)	0.046(4)	0.000(3)	0.006(4)	0.015(3)
C8	0.032(4)	0.034(4)	0.041(4)	0.009(3)	0.010(3)	0.008(3)
C9	0.047(4)	0.029(3)	0.025(3)	0.006(3)	0.003(3)	0.001(3)
C10	0.043(4)	0.036(4)	0.024(3)	0.005(3)	0.006(3)	0.001(3)
C11	0.048(4)	0.060(5)	0.061(5)	0.006(4)	0.028(4)	0.010(4)
C12	0.058(5)	0.040(4)	0.055(4)	-0.001(3)	0.006(4)	-0.018(3)
C13	0.058(5)	0.045(4)	0.045(4)	-0.008(3)	-0.005(4)	-0.003(3)
C14	0.049(4)	0.055(4)	0.027(3)	0.002(3)	0.007(3)	0.007(3)
C15	0.040(4)	0.039(4)	0.039(4)	0.004(3)	0.010(3)	0.013(3)
C16	0.049(4)	0.042(4)	0.046(4)	-0.014(3)	0.005(3)	-0.001(3)
C17	0.035(4)	0.044(4)	0.047(4)	-0.007(3)	0.007(3)	0.001(3)
N1	0.036(3)	0.025(3)	0.025(3)	-0.001(2)	0.002(2)	0.000(2)
N2	0.035(3)	0.030(3)	0.039(3)	0.001(2)	0.010(3)	0.006(2)
N3	0.030(3)	0.029(3)	0.038(3)	0.008(2)	0.003(2)	0.000(2)
N4	0.041(3)	0.027(3)	0.032(3)	-0.002(2)	-0.001(2)	0.001(2)
N5	0.032(3)	0.035(3)	0.029(3)	-0.004(2)	0.006(2)	0.006(2)
O1	0.033(3)	0.052(3)	0.052(3)	-0.003(2)	0.016(2)	-0.008(2)
O2	0.061(3)	0.058(3)	0.057(3)	-0.015(3)	0.032(3)	-0.002(2)
O3	0.038(3)	0.052(3)	0.058(3)	0.006(2)	0.021(2)	0.002(2)
O4	0.058(3)	0.048(3)	0.042(3)	-0.009(2)	0.021(2)	-0.004(2)

Table S7 Crystal data and structure refinement for complex **3b**.

Chemical formula	C ₁₈ H ₂₇ N ₅ NiO ₄		
Formula weight	436.15 g/mol		
Temperature	103(2) K		
Wavelength	0.71073 Å		
Crystal size	0.020 x 0.200 x 0.400 mm		
Crystal habit	red plate		
Crystal system	monoclinic		
Space group	C 1 2/c 1		
Unit cell dimensions	a = 25.970(3) Å	α = 90°	
	b = 8.6558(7) Å	β = 105.855(3)°	
	c = 18.0823(17) Å	γ = 90°	
Volume	3910.1(6) Å ³		
Z	8		
Density (calculated)	1.482 g/cm ³		
Absorption coefficient	1.027 mm ⁻¹		
F(000)	1840		
Theta range for data collection	1.63 to 30.07°		
Index ranges	-36 ≤ h ≤ 36, -12 ≤ k ≤ 12, -25 ≤ l ≤ 25		
Reflections collected	24374		
Independent reflections	5732 [R(int) = 0.1248]		
Coverage of independent reflections	99.7%		
Absorption correction	Multi-Scan		
Max. and min. transmission	0.9800 and 0.6840		
Structure solution technique	direct methods		
Structure solution program	XT, VERSION 2014/4		
Refinement method	Full-matrix least-squares on F ²		
Refinement program	SHELXL-2014/7 (Sheldrick, 2014)		
Function minimized	Σ w(F _o ² - F _c ²) ²		
Data / restraints / parameters	5732 / 0 / 260		
Goodness-of-fit on F²	0.988		
Final R indices	2854 data; R1 = 0.0668, wR2 = 0.1329 I > 2σ(I)		
	all data R1 = 0.1674, wR2 = 0.1688		
Weighting scheme	w = 1/[σ ² (F _o ²) + (0.0712P) ²] where P = (F _o ² + 2F _c ²)/3		
Largest diff. peak and hole	1.469 and -0.516 eÅ ⁻³		
R.M.S. deviation from mean	0.121 eÅ ⁻³		

Table S8 Selected bond lengths (Å) for complex **3b**.

Ni1-N1	1.838(3)	Ni1-N2	1.847(3)
Ni1-N4	1.904(4)	Ni1-N3	1.924(3)
C7-O1	1.239(5)	C7-N2	1.332(5)

C7-C8	1.509(6)	C8-N3	1.300(5)
C8-O2	1.334(5)	C9-O2	1.461(5)
C9-C10	1.500(7)	C13-O3	1.263(5)
C13-N4	1.319(5)	C13-C14	1.535(6)
C14-O4	1.235(5)	C14-N1	1.338(5)

Table S9 Selected bond angles (°) for complex **3b**.

N1-Ni1-N2	85.08(15)	N1-Ni1-N4	84.45(15)
N2-Ni1-N4	169.41(14)	N1-Ni1-N3	168.55(15)
N2-Ni1-N3	83.49(14)	N4-Ni1-N3	106.99(15)
C6-C1-N1	113.6(4)	C1-C6-N2	113.1(4)
N1-C1-C2	126.6(4)	N2-C6-C5	126.5(4)
O1-C7-N2	129.5(4)	O1-C7-C8	122.8(4)
N2-C7-C8	107.7(4)	N3-C8-O2	118.3(4)
N3-C8-C7	117.2(4)	O2-C8-C7	124.5(4)
O2-C9-C10	105.2(4)	O3-C13-N4	127.8(4)
O3-C13-C14	118.3(4)	N4-C13-C14	113.9(4)
O4-C14-N1	128.1(4)	O4-C14-C13	122.4(4)
N1-C14-C13	109.5(4)	C14-N1-C1	127.6(4)
C14-N1-Ni1	118.1(3)	C1-N1-Ni1	114.2(3)
C7-N2-C6	126.7(4)	C7-N2-Ni1	119.2(3)
C6-N2-Ni1	114.0(3)	C8-N3-C11	119.1(4)
C8-N3-Ni1	112.3(3)	C11-N3-Ni1	128.6(3)
C13-N4-C12	116.7(4)	C13-N4-Ni1	114.0(3)
C12-N4-Ni1	129.3(3)	C8-O2-C9	122.5(3)

Table S10 Atomic coordinates and equivalent isotropic atomic displacement parameters (\AA^2) for complex **3b**.

U(eq) is defined as one third of the trace of the orthogonalized U_{ij} tensor.

	x/a	y/b	z/c	U(eq)
Ni1	0.71789(2)	0.54657(6)	0.49808(3)	0.02072(16)
C1	0.67193(17)	0.7371(5)	0.5826(2)	0.0263(10)
C2	0.63550(17)	0.8281(5)	0.6099(3)	0.0293(10)
C3	0.65348(19)	0.9026(5)	0.6800(3)	0.0325(11)
C4	0.70656(18)	0.8912(5)	0.7230(3)	0.0322(11)
C5	0.74233(17)	0.8039(5)	0.6963(2)	0.0266(10)
C6	0.72454(16)	0.7264(4)	0.6252(3)	0.0239(10)
C7	0.80838(16)	0.6098(5)	0.6152(2)	0.0218(9)
C8	0.82394(16)	0.5026(4)	0.5590(2)	0.0218(9)
C9	0.91755(17)	0.4807(6)	0.6348(3)	0.0351(11)
C10	0.96442(19)	0.3947(7)	0.6217(3)	0.0600(17)
C11	0.79902(17)	0.3505(5)	0.4450(3)	0.0322(11)
C12	0.67551(18)	0.3641(5)	0.3497(2)	0.0338(11)
C13	0.61892(17)	0.5290(5)	0.3969(3)	0.0281(10)
C14	0.61298(16)	0.6370(5)	0.4614(3)	0.0275(10)
C15	0.45844(19)	0.4700(6)	0.3593(4)	0.0554(16)
C16	0.44372(18)	0.6868(7)	0.4398(3)	0.0528(16)
C17	0.37372(16)	0.6122(6)	0.3261(3)	0.0385(12)
C18	0.45496(17)	0.7311(5)	0.3124(3)	0.0335(11)
N1	0.66032(13)	0.6517(4)	0.5139(2)	0.0243(8)
N2	0.75579(12)	0.6333(4)	0.59020(19)	0.0205(7)
N3	0.78602(13)	0.4569(4)	0.50004(19)	0.0222(7)
N4	0.66754(13)	0.4723(4)	0.4078(2)	0.0248(8)
N5	0.43265(13)	0.6245(4)	0.3597(2)	0.0302(9)
O1	0.84105(11)	0.6600(3)	0.67359(17)	0.0291(7)
O2	0.87361(11)	0.4527(3)	0.56599(16)	0.0282(7)
O3	0.57837(13)	0.5051(4)	0.34094(19)	0.0423(9)
O4	0.56957(12)	0.6939(4)	0.46245(19)	0.0399(8)

Table S11 Anisotropic atomic displacement parameters (\AA^2) for complex **3b**.

The anisotropic atomic displacement factor exponent takes the form:

$$-2\pi^2[h^2 a^{*2} U_{11} + \dots + 2 h k a^* b^* U_{12}]$$

	U_{11}	U_{22}	U_{33}	U_{23}	U_{13}	U_{12}
Ni1	0.0177(3)	0.0211(3)	0.0228(3)	0.0051(3)	0.0046(2)	-0.0005(2)
C1	0.033(3)	0.022(2)	0.025(2)	0.0092(19)	0.010(2)	-0.0100(19)
C2	0.023(2)	0.026(3)	0.040(3)	0.008(2)	0.010(2)	-0.0001(18)
C3	0.041(3)	0.025(3)	0.040(3)	0.003(2)	0.026(2)	0.005(2)
C4	0.041(3)	0.028(3)	0.031(3)	-0.001(2)	0.014(2)	0.000(2)
C5	0.026(2)	0.026(2)	0.027(3)	0.0033(19)	0.0048(19)	0.0015(18)
C6	0.030(2)	0.015(2)	0.034(3)	0.0102(19)	0.022(2)	0.0039(17)
C7	0.022(2)	0.018(2)	0.025(2)	0.0036(18)	0.0062(18)	-0.0035(17)
C8	0.020(2)	0.019(2)	0.025(2)	0.0099(17)	0.0055(18)	0.0016(15)
C9	0.028(2)	0.036(3)	0.036(3)	-0.002(2)	-0.001(2)	-0.002(2)
C10	0.028(3)	0.064(4)	0.076(5)	-0.020(3)	-0.007(3)	0.011(3)
C11	0.027(2)	0.036(3)	0.033(3)	-0.001(2)	0.008(2)	0.003(2)
C12	0.034(3)	0.033(3)	0.029(3)	-0.003(2)	0.001(2)	-0.006(2)
C13	0.025(2)	0.025(2)	0.031(3)	0.006(2)	0.0034(19)	-0.0047(19)
C14	0.019(2)	0.026(3)	0.036(3)	0.008(2)	0.0047(19)	-0.0041(18)
C15	0.029(3)	0.032(3)	0.100(5)	0.018(3)	0.009(3)	0.008(2)
C16	0.023(3)	0.106(5)	0.029(3)	-0.002(3)	0.006(2)	-0.002(3)
C17	0.017(2)	0.047(3)	0.046(3)	0.007(3)	0.001(2)	-0.005(2)
C18	0.028(2)	0.037(3)	0.036(3)	0.009(2)	0.008(2)	-0.001(2)
N1	0.0183(17)	0.025(2)	0.029(2)	0.0076(16)	0.0058(15)	0.0018(15)
N2	0.0186(17)	0.0169(18)	0.0255(19)	0.0040(15)	0.0054(14)	0.0002(14)
N3	0.0254(17)	0.0205(18)	0.0215(17)	0.0035(17)	0.0078(14)	-0.0003(16)
N4	0.0235(18)	0.023(2)	0.027(2)	0.0037(16)	0.0049(15)	-0.0002(15)
N5	0.0187(18)	0.038(2)	0.032(2)	0.0104(18)	0.0044(16)	0.0020(16)
O1	0.0228(15)	0.0319(18)	0.0305(18)	-0.0002(14)	0.0037(14)	0.0011(13)
O2	0.0177(14)	0.0323(17)	0.0326(17)	-0.0022(15)	0.0038(12)	0.0003(13)
O3	0.0277(18)	0.055(2)	0.037(2)	-0.0038(16)	-0.0027(15)	-0.0073(15)
O4	0.0181(16)	0.046(2)	0.052(2)	0.0004(16)	0.0033(15)	-0.0001(14)

Table S12 Crystal data and structure refinement for complex **3c**.

Chemical formula	C ₁₉ H ₂₉ N ₅ NiO ₄	
Formula weight	450.18 g/mol	
Temperature	103(2) K	
Wavelength	1.54178 Å	
Crystal size	0.005 x 0.100 x 0.140 mm	
Crystal habit	red plate	
Crystal system	monoclinic	
Space group	P 1 21/c 1	
Unit cell dimensions	a = 15.8813(4) Å	α = 90°
	b = 24.8528(6) Å	β = 94.7164(15)°
	c = 10.6517(3) Å	γ = 90°
Volume	4189.93(19) Å ³	
Z	8	
Density (calculated)	1.427 g/cm ³	
Absorption coefficient	1.636 mm ⁻¹	
F(000)	1904	
Theta range for data collection	2.79 to 66.65°	
Reflections collected	7340	
Coverage of independent reflections	99.1%	
Absorption correction	Multi-Scan	
Max. and min. transmission	0.9920 and 0.8030	
Refinement method	Full-matrix least-squares on F ²	
Refinement program	SHELXL-2014/7 (Sheldrick, 2014)	
Function minimized	Σ w(F _o ² - F _c ²) ²	
Data / restraints / parameters	7340 / 0 / 539	
Goodness-of-fit on F²	1.087	
Δ/σ_{max}	0.002	
Final R indices	6483 data; I > 2σ(I)	R1 = 0.0459, wR2 = 0.1189
	all data	R1 = 0.0551, wR2 = 0.1239
Weighting scheme	w = 1/[σ ² (F _o ²) + (0.0546P) ² + 4.8171P] where P = (F _o ² + 2F _c ²)/3	
Largest diff. peak and hole	0.403 and -0.413 eÅ ⁻³	
R.M.S. deviation from mean	0.062 eÅ ⁻³	

Table S13 Selected bond lengths (Å) for complex **3c**.

Ni1-N2	1.845(2)	Ni1-N3	1.849(2)
Ni1-N1	1.909(2)	Ni1-N4	1.927(2)
C2-N1	1.333(4)	C2-O1	1.250(3)
C3-O2	1.240(3)	C2-C3	1.531(4)
C4-N2	1.405(3)	C3-N2	1.334(3)
C10-O3	1.239(3)	C9-N3	1.404(3)
C10-C11	1.525(4)	C10-N3	1.328(3)
C11-O4	1.331(3)	C11-N4	1.293(3)
C13-O4	1.483(3)	C12-N4	1.467(3)
C13-C14	1.514(4)	C13-C15	1.505(4)

Table S14 Selected bond angles (°) for complex **3c**.

N2-Ni1-N3	84.49(9)	N2-Ni1-N1	84.51(10)
N3-Ni1-N1	168.68(10)	N2-Ni1-N4	168.08(10)
N3-Ni1-N4	83.59(9)	N1-Ni1-N4	107.41(10)
O1-C2-N1	127.8(3)	O1-C2-C3	118.7(2)
N1-C2-C3	113.6(2)	O2-C3-N2	128.0(3)
O2-C3-C2	121.8(2)	N2-C3-C2	110.2(2)
C5-C4-C9	119.7(2)	C5-C4-N2	127.5(2)
C9-C4-N2	112.8(2)	N3-C9-C4	112.4(2)
O3-C10-N3	129.3(3)	O3-C10-C11	122.5(2)
N3-C10-C11	108.2(2)	N4-C11-O4	119.9(3)
N4-C11-C10	116.4(2)	O4-C11-C10	123.7(2)
O4-C13-C15	108.7(2)	O4-C13-C14	103.5(2)
C15-C13-C14	112.3(2)	C2-N1-Ni1	113.64(19)
C2-N1-C1	116.0(2)	C3-N2-C4	126.6(2)
C1-N1-Ni1	130.36(18)	C4-N2-Ni1	115.08(16)
C3-N2-Ni1	117.73(19)	C10-N3-Ni1	118.90(18)
C10-N3-C9	125.9(2)	C11-N4-C12	119.6(2)
C9-N3-Ni1	115.22(17)	C12-N4-Ni1	127.61(17)
C11-N4-Ni1	112.76(19)	C11-O4-C13	122.9(2)

Table S15 Atomic coordinates and equivalent isotropic atomic displacement parameters (\AA^2) for complex **3c**.U(eq) is defined as one third of the trace of the orthogonalized U_{ij} tensor.

	x/a	y/b	z/c	U(eq)
H1A	0.2198	0.6102	1.2717	0.051
H1B	0.2674	0.5644	1.1990	0.051
H1C	0.1918	0.5486	1.2824	0.051
H5	-0.0869	0.6421	0.7977	0.034
H6	-0.1590	0.6128	0.6096	0.041
H7	-0.1254	0.5311	0.5196	0.043
H8	-0.0239	0.4740	0.6243	0.039
H12A	0.2604	0.4187	1.1158	0.051
H12B	0.2228	0.4653	1.1985	0.051
H12C	0.2947	0.4791	1.1066	0.051
H13	0.0992	0.3377	0.8613	0.034
H14A	0.2449	0.2894	0.9944	0.054
H14B	0.1641	0.2557	0.9400	0.054
H14C	0.1558	0.2980	1.0515	0.054
H15A	0.1873	0.3546	0.6990	0.054
H15B	0.1844	0.2910	0.7209	0.054
H15C	0.2647	0.3250	0.7761	0.054
H16A	0.2537	0.5784	0.7075	0.052
H16B	0.3088	0.5245	0.7230	0.052
H16C	0.2266	0.5263	0.6255	0.052
H20	0.5146	0.6654	0.2764	0.035
H21	0.5962	0.6487	0.1080	0.038
H22	0.6072	0.5622	0.0275	0.038
H23	0.5429	0.4895	0.1219	0.035
H27A	0.3119	0.3871	0.5700	0.045
H27B	0.2512	0.4386	0.5607	0.045
H27C	0.3334	0.4382	0.6584	0.045
H28	0.4786	0.3347	0.3254	0.038
H29A	0.4517	0.2836	0.5039	0.064
H29B	0.4476	0.2451	0.3833	0.064
H29C	0.3622	0.2653	0.4379	0.064
H30A	0.3112	0.3083	0.2280	0.069
H30B	0.3936	0.2839	0.1724	0.069
H30C	0.3749	0.3471	0.1620	0.069
H31A	0.1946	0.7061	0.4964	0.053
H31B	0.1269	0.7515	0.4533	0.053
H31C	0.1408	0.7013	0.3631	0.053
H32A	0.0481	0.6038	0.5498	0.061
H32B	0.1469	0.6175	0.5592	0.061
H32C	0.0956	0.6116	0.4242	0.061
H33A	0.0252	0.6840	0.6834	0.072
H33B	0.0590	0.7413	0.6409	0.072
H33C	0.1246	0.6956	0.6900	0.072
H34A	-0.0069	0.6790	0.3516	0.068
H34B	-0.0238	0.7298	0.4384	0.068

H34C	-0.0543	0.6711	0.4772	0.068
H35A	0.2712	0.7322	0.8674	0.064
H35B	0.2183	0.6819	0.9122	0.064
H35C	0.2736	0.6761	0.7940	0.064
H36A	0.4223	0.6736	0.8193	0.057
H36B	0.4724	0.6769	0.9557	0.057
H36C	0.4269	0.7293	0.8948	0.057
H37A	0.3504	0.5982	0.8986	0.057
H37B	0.2887	0.6051	1.0090	0.057
H37C	0.3889	0.6051	1.0413	0.057
H38A	0.3895	0.6928	1.1432	0.057
H38B	0.2885	0.6935	1.1235	0.057
H38C	0.3417	0.7426	1.0738	0.057

Table S16 Anisotropic atomic displacement parameters (\AA^2) for complex **3c**.

The anisotropic atomic displacement factor exponent takes the form:

$$-2\pi^2 [h^2 a^{*2} U_{11} + \dots + 2 h k a^* b^* U_{12}]$$

	U_{11}	U_{22}	U_{33}	U_{23}	U_{13}	U_{12}
Ni1	0.0234(2)	0.0231(2)	0.0234(2)	-0.00158(16)	0.00159(18)	-0.00106(16)
Ni2	0.0239(2)	0.0227(2)	0.0253(3)	-0.00171(16)	-0.00141(18)	0.00189(16)
C1	0.0363(17)	0.0360(15)	0.0289(16)	-0.0045(11)	-0.0040(12)	0.0000(12)
C2	0.0278(15)	0.0296(14)	0.0322(16)	-0.0045(11)	0.0046(12)	-0.0029(10)
C3	0.0222(14)	0.0268(14)	0.0311(15)	-0.0021(10)	0.0061(11)	-0.0019(10)
C4	0.0224(14)	0.0256(13)	0.0252(14)	0.0016(10)	0.0025(10)	-0.0050(9)
C5	0.0242(14)	0.0281(14)	0.0328(15)	0.0003(10)	0.0020(11)	-0.0011(10)
C6	0.0299(16)	0.0319(15)	0.0391(17)	0.0026(11)	-0.0031(12)	0.0016(11)
C7	0.0348(17)	0.0391(16)	0.0317(16)	-0.0016(12)	-0.0069(12)	-0.0003(12)
C8	0.0343(16)	0.0277(14)	0.0336(16)	-0.0034(11)	-0.0041(12)	-0.0017(11)
C9	0.0236(14)	0.0263(13)	0.0270(14)	0.0027(10)	0.0009(11)	-0.0044(10)
C10	0.0356(16)	0.0256(14)	0.0304(15)	0.0000(11)	-0.0012(12)	0.0003(11)
C11	0.0355(16)	0.0218(13)	0.0274(15)	-0.0002(10)	0.0027(12)	-0.0003(10)
C12	0.0339(16)	0.0333(15)	0.0326(16)	-0.0021(11)	-0.0059(12)	0.0046(11)
C13	0.0273(15)	0.0245(13)	0.0339(16)	-0.0028(10)	-0.0007(11)	-0.0008(10)
C14	0.0349(17)	0.0319(15)	0.0416(18)	0.0036(12)	0.0046(13)	0.0046(11)
C15	0.0291(16)	0.0440(17)	0.0352(17)	-0.0039(12)	0.0026(12)	-0.0008(12)
C16	0.0365(17)	0.0357(15)	0.0312(16)	-0.0033(11)	0.0038(12)	0.0044(12)
C17	0.0258(15)	0.0311(14)	0.0317(15)	-0.0071(11)	-0.0089(11)	0.0049(11)
C18	0.0256(15)	0.0236(14)	0.0344(16)	-0.0054(10)	-0.0074(11)	0.0025(10)
C19	0.0219(13)	0.0271(13)	0.0273(14)	-0.0004(10)	-0.0040(11)	0.0005(10)
C20	0.0279(15)	0.0235(13)	0.0345(16)	0.0006(10)	-0.0055(12)	0.0002(10)
C21	0.0279(15)	0.0301(14)	0.0368(16)	0.0077(11)	-0.0033(12)	-0.0042(11)
C22	0.0307(16)	0.0360(15)	0.0291(16)	0.0031(11)	0.0010(12)	-0.0005(11)
C23	0.0330(16)	0.0257(13)	0.0289(15)	0.0005(10)	-0.0014(12)	0.0002(10)
C24	0.0260(14)	0.0247(13)	0.0252(14)	0.0018(10)	-0.0065(11)	0.0002(10)
C25	0.0345(16)	0.0264(14)	0.0249(14)	-0.0011(10)	0.0008(11)	0.0002(11)
C26	0.0319(15)	0.0257(13)	0.0227(14)	0.0012(10)	-0.0014(11)	0.0002(10)

C27	0.0252(15)	0.0331(14)	0.0331(16)	0.0034(11)	0.0052(11)	0.0003(10)
C28	0.0383(17)	0.0220(13)	0.0354(16)	-0.0015(10)	0.0040(13)	0.0005(11)
C29	0.0439(19)	0.0303(16)	0.052(2)	0.0077(13)	-0.0028(15)	-0.0045(12)
C30	0.048(2)	0.0488(19)	0.0403(19)	-0.0039(14)	-0.0017(15)	-0.0014(14)
C31	0.0328(16)	0.0332(15)	0.0399(17)	0.0029(12)	0.0062(13)	-0.0020(11)
C32	0.0373(18)	0.0285(15)	0.056(2)	0.0023(13)	-0.0019(15)	0.0022(12)
C33	0.070(2)	0.0412(18)	0.0336(18)	-0.0054(13)	0.0102(16)	-0.0189(16)
C34	0.0324(17)	0.0344(16)	0.067(2)	0.0018(14)	-0.0126(16)	-0.0020(12)
C35	0.0364(18)	0.059(2)	0.0322(17)	-0.0052(13)	-0.0003(14)	0.0133(14)
C36	0.0366(17)	0.0305(15)	0.0487(19)	-0.0012(12)	0.0128(14)	-0.0024(12)
C37	0.0319(17)	0.0331(15)	0.0497(19)	-0.0049(12)	0.0071(14)	-0.0050(12)
C38	0.0397(18)	0.0431(17)	0.0298(16)	-0.0062(12)	-0.0004(13)	0.0068(13)
N1	0.0246(12)	0.0294(12)	0.0258(12)	-0.0020(8)	0.0015(9)	-0.0009(9)
N2	0.0230(12)	0.0244(11)	0.0257(12)	-0.0004(8)	0.0018(9)	-0.0013(8)
N3	0.0261(12)	0.0229(11)	0.0255(12)	0.0003(8)	0.0013(9)	-0.0015(8)
N4	0.0253(12)	0.0287(11)	0.0238(12)	0.0013(8)	0.0009(9)	-0.0006(8)
N5	0.0237(12)	0.0300(12)	0.0274(12)	-0.0025(9)	-0.0039(9)	0.0022(8)
N6	0.0261(12)	0.0237(11)	0.0283(12)	-0.0013(8)	-0.0032(9)	0.0003(8)
N7	0.0253(12)	0.0233(11)	0.0250(12)	0.0010(8)	-0.0023(9)	-0.0003(8)
N8	0.0238(12)	0.0270(11)	0.0253(12)	0.0034(8)	0.0003(9)	0.0023(8)
N9	0.0264(13)	0.0286(12)	0.0299(13)	-0.0014(9)	-0.0007(10)	-0.0026(9)
N10	0.0265(13)	0.0355(13)	0.0300(13)	-0.0041(9)	0.0036(10)	0.0035(9)
O1	0.0488(14)	0.0309(11)	0.0443(13)	-0.0126(9)	-0.0104(10)	0.0016(9)
O2	0.0325(11)	0.0262(10)	0.0463(13)	-0.0058(8)	-0.0022(9)	0.0028(8)
O3	0.0679(16)	0.0276(10)	0.0399(13)	-0.0107(9)	-0.0219(11)	0.0114(10)
O4	0.0420(13)	0.0264(10)	0.0420(12)	-0.0065(8)	-0.0129(10)	0.0061(8)
O5	0.0383(12)	0.0336(11)	0.0397(12)	-0.0096(8)	0.0039(9)	0.0064(8)
O6	0.0372(12)	0.0239(10)	0.0494(13)	-0.0050(8)	0.0028(10)	0.0003(8)
O7	0.0763(17)	0.0241(10)	0.0382(12)	-0.0033(8)	0.0256(11)	-0.0029(10)
O8	0.0634(16)	0.0249(10)	0.0420(13)	-0.0009(8)	0.0235(11)	-0.0027(9)

Table S17 Crystal data and structure refinement for complex **3d**.

Chemical formula	C ₂₀ H ₃₁ N ₅ NiO ₄	
Formula weight	464.21 g/mol	
Temperature	153(2) K	
Wavelength	0.71073 Å	
Crystal size	0.040 x 0.320 x 0.420 mm	
Crystal habit	red plate	
Crystal system	monoclinic	
Space group	P 1 21/c 1	
Unit cell dimensions	a = 19.1442(14) Å	α = 90°
	b = 10.1337(7) Å	β = 102.976(2)°
	c = 11.8238(8) Å	γ = 90°
Volume	2235.3(3) Å ³	
Z	4	
Density (calculated)	1.379 g/cm ³	
Absorption coefficient	0.903 mm ⁻¹	
F(000)	984	
Theta range for data collection	2.18 to 31.12°	
Index ranges	-27 ≤ h ≤ 27, -14 ≤ k ≤ 14, -17 ≤ l ≤ 15	
Reflections collected	43588	
Independent reflections	7173 [R(int) = 0.0851]	
Coverage of independent reflections	99.6%	
Absorption correction	Multi-Scan	
Max. and min. transmission	0.9650 and 0.7030	
Structure solution technique	direct methods	
Structure solution program	XS, VERSION 2013/1	
Refinement method	Full-matrix least-squares on F ²	
Refinement program	SHELXL-2014/7 (Sheldrick, 2014)	
Function minimized	Σ w(F _o ² - F _c ²) ²	
Data / restraints / parameters	7173 / 200 / 327	
Goodness-of-fit on F²	1.010	
Δ/σ_{max}	0.001	
Final R indices	4017 data;	R1 = 0.0529, wR2 = 0.1212
	I > 2σ(I)	
	all data	R1 = 0.1209, wR2 = 0.1519
Weighting scheme	w = 1/[σ ² (F _o ²) + (0.0599P) ² + 1.5960P] where P = (F _o ² + 2F _c ²)/3	
Largest diff. peak and hole	0.507 and -0.554 eÅ ⁻³	
R.M.S. deviation from mean	0.076 eÅ ⁻³	

Table S18 Selected bond lengths (Å) for complex **3d**.

Ni1-N3	1.835(2)	Ni1-N2	1.844(2)
Ni1-N4	1.899(3)	Ni1-N1	1.926(3)
C1-N1	1.469(4)	C2-N1	1.299(5)
C2-O1	1.315(18)	C2-C3	1.514(5)
C3-N2	1.341(4)	C3-O2	1.227(4)
C4-N3	1.334(4)	C4-O3	1.233(3)
C5-O4	1.246(4)	C4-C5	1.536(4)
C6-N4	1.467(4)	C5-N4	1.328(4)
C7-C8	1.501(15)	O1-C7	1.573(15)
C8-C9	1.531(16)	C8-C10	1.474(16)

Table S19 Selected bond angles (°) for complex **3d**.

N3-Ni1-N2	84.59(10)	N3-Ni1-N4	84.30(11)
N2-Ni1-N4	168.84(11)	N3-Ni1-N1	167.93(11)
N2-Ni1-N1	83.43(12)	N4-Ni1-N1	107.70(12)
N1-C2-O1	110.1(8)	N1-C2-O1A	123.5(4)
N1-C2-C3	117.5(3)	O1-C2-C3	131.7(9)
O2-C3-C2	122.8(3)	O2-C3-N2	130.1(3)
O3-C4-N3	128.4(3)	N2-C3-C2	107.1(3)
N3-C4-C5	109.9(3)	O3-C4-C5	121.7(3)
O4-C5-C4	118.7(3)	O4-C5-N4	128.4(3)
C16-C11-N2	112.1(2)	N4-C5-C4	112.9(3)
C12-C11-N2	127.4(3)	C15-C16-N3	127.5(3)
C11-C16-N3	112.6(2)	C2-O1-C7	122.7(14)
C8-C7-O1	97.7(13)	C10-C8-C7	104.5(15)
C10-C8-C9	108.3(18)	C7-C8-C9	113.5(17)
C2-N1-C1	117.7(3)	C2-N1-Ni1	112.4(2)
C1-N1-Ni1	130.0(3)	C3-N2-C11	125.0(3)
C3-N2-Ni1	119.7(2)	C11-N2-Ni1	115.31(19)
C4-N3-C16	126.3(2)	C4-N3-Ni1	118.35(19)
C16-N3-Ni1	115.33(19)	C5-N4-C6	116.4(3)
C5-N4-Ni1	114.54(19)	C6-N4-Ni1	129.0(2)

Table S20 Atomic coordinates and equivalent isotropic atomic displacement parameters (\AA^2) for complex **3d**.

$U(\text{eq})$ is defined as one third of the trace of the orthogonalized U_{ij} tensor.

	x/a	y/b	z/c	U(eq)
H1A	0.4525	0.6978	0.3979	0.094
H1B	0.3727	0.6476	0.3940	0.094
H1C	0.4075	0.7609	0.4833	0.094
H6A	0.2169	0.7527	0.5335	0.075
H6B	0.2982	0.7998	0.5468	0.075
H6C	0.2679	0.6783	0.4638	0.075
H12	0.3262	1.1334	-0.0277	0.047
H13	0.2359	1.2744	-0.1275	0.053
H14	0.1299	1.3014	-0.0664	0.049
H15	0.1096	1.1830	0.0926	0.042
H17A	0.1731	0.5668	0.1476	0.066
H17B	0.1902	0.4943	0.2710	0.066
H17C	0.1887	0.6520	0.2645	0.066
H18A	0.0981	0.6565	0.3857	0.066
H18B	0.1042	0.4991	0.3927	0.066
H18C	0.0276	0.5675	0.3479	0.066
H19A	0.0042	0.4482	0.1619	0.066
H19B	0.0768	0.3694	0.2137	0.066
H19C	0.0658	0.4411	0.0904	0.066
H20A	0.0725	0.7673	0.2014	0.059
H20B	0.0011	0.6818	0.1591	0.059
H20C	0.0604	0.6854	0.0829	0.059
H7A	0.5558	0.7533	0.1843	0.083
H7B	0.5301	0.9045	0.1567	0.083
H8	0.6186	0.8075	0.3711	0.087
H9A	0.6614	0.9310	0.1993	0.138
H9B	0.7084	0.9202	0.3292	0.138
H9C	0.6592	1.0472	0.2901	0.138
H10A	0.5458	1.0526	0.3249	0.132
H10B	0.5993	1.0160	0.4454	0.132
H10C	0.5252	0.9379	0.4046	0.132
H7A1	0.5548	0.8763	0.1588	0.075
H7A2	0.5260	0.9881	0.2338	0.075
H8A	0.6032	0.7664	0.3451	0.072
H9A1	0.6825	0.8571	0.2463	0.111
H9A2	0.7079	0.9120	0.3760	0.111
H9A3	0.6627	1.0045	0.2761	0.111
H10D	0.5780	1.0218	0.4265	0.121
H10E	0.6315	0.9179	0.5032	0.121
H10F	0.5477	0.8855	0.4645	0.121

Table S21 Anisotropic atomic displacement parameters (\AA^2) for complex **3d**.

The anisotropic atomic displacement factor exponent takes the form:

$$-2\pi^2 [h^2 a^{*2} U_{11} + \dots + 2 h k a^* b^* U_{12}]$$

	U_{11}	U_{22}	U_{33}	U_{23}	U_{13}	U_{12}
Ni1	0.0404(2)	0.02771(19)	0.02737(19)	-0.00049(15)	0.00124(14)	0.00289(16)
C1	0.064(3)	0.053(2)	0.065(2)	0.0089(18)	0.0017(19)	0.0124(18)
C2	0.0379(18)	0.0422(18)	0.058(2)	-0.0054(16)	-0.0013(16)	0.0048(14)
C3	0.0424(18)	0.0381(16)	0.0433(18)	-0.0039(14)	0.0026(15)	0.0031(14)
C4	0.0400(16)	0.0279(14)	0.0294(14)	-0.0080(11)	0.0056(12)	-0.0021(12)
C5	0.0466(18)	0.0337(15)	0.0267(13)	-0.0024(12)	0.0063(12)	-0.0077(14)
C6	0.062(2)	0.0463(19)	0.0369(17)	0.0102(14)	0.0020(16)	0.0018(16)
C11	0.0383(15)	0.0275(13)	0.0269(13)	-0.0049(11)	0.0036(11)	0.0009(12)
C12	0.0471(18)	0.0384(16)	0.0339(15)	-0.0016(12)	0.0122(13)	-0.0016(14)
C13	0.060(2)	0.0381(17)	0.0342(16)	0.0078(13)	0.0098(15)	-0.0019(15)
C14	0.0484(19)	0.0305(15)	0.0404(17)	0.0064(12)	0.0025(14)	0.0039(13)
C15	0.0402(16)	0.0276(14)	0.0355(15)	-0.0016(11)	0.0050(12)	0.0021(12)
C16	0.0371(15)	0.0229(12)	0.0258(12)	-0.0049(10)	0.0041(11)	-0.0005(11)
C17	0.0343(16)	0.051(2)	0.0456(18)	-0.0032(15)	0.0056(13)	0.0068(14)
C18	0.0505(19)	0.0509(19)	0.0295(15)	-0.0002(13)	0.0081(13)	0.0073(15)
C19	0.050(2)	0.0348(16)	0.0471(19)	-0.0120(13)	0.0106(15)	0.0012(13)
C20	0.0439(18)	0.0349(16)	0.0365(16)	0.0007(12)	0.0036(13)	0.0061(13)
O1	0.058(4)	0.080(5)	0.082(5)	0.009(5)	-0.002(5)	0.013(4)
C7	0.055(4)	0.075(4)	0.072(4)	0.010(4)	0.001(4)	0.006(4)
C8	0.061(4)	0.079(5)	0.076(5)	0.012(4)	0.010(4)	0.000(4)
C9	0.071(8)	0.099(10)	0.100(10)	0.016(9)	0.007(8)	0.000(8)
C10	0.068(7)	0.079(8)	0.112(8)	0.005(7)	0.013(7)	0.006(7)
O1A	0.0375(19)	0.067(2)	0.053(3)	0.005(2)	0.005(2)	0.0138(17)
C7A	0.038(2)	0.069(3)	0.078(3)	0.018(3)	0.007(2)	0.006(2)
C8A	0.050(3)	0.067(3)	0.064(3)	0.020(3)	0.012(2)	0.006(2)
C9A	0.048(3)	0.101(6)	0.072(4)	0.046(4)	0.013(3)	0.012(3)
C10A	0.072(4)	0.091(5)	0.082(5)	-0.033(4)	0.025(4)	-0.013(4)
N1	0.0492(16)	0.0338(13)	0.0430(15)	0.0008(11)	-0.0083(12)	0.0061(12)
N2	0.0356(13)	0.0328(13)	0.0330(12)	-0.0027(10)	0.0049(10)	0.0038(10)
N3	0.0400(14)	0.0272(12)	0.0261(11)	-0.0020(9)	0.0040(10)	0.0011(10)
N4	0.0497(16)	0.0321(13)	0.0273(12)	0.0019(10)	0.0036(11)	0.0003(11)
N5	0.0334(13)	0.0336(13)	0.0313(12)	-0.0041(9)	0.0031(10)	0.0049(10)
O2	0.0445(14)	0.0651(17)	0.0618(16)	0.0021(13)	0.0211(12)	0.0087(12)
O3	0.0396(12)	0.0449(12)	0.0387(12)	0.0011(9)	0.0098(9)	0.0022(10)
O4	0.0533(14)	0.0573(15)	0.0369(12)	0.0069(10)	0.0134(11)	-0.0084(11)

References

1. Garrido, B.; Garrido Barros, P.; Funes Ardoiz, I.; Drouet, S.; Benet Buchholz, J.; Maseras, F.; Llobet, A. *J. Am. Chem. Soc.* **2015**, *137*, 6758-6761.
2. SMART version 5.628; Bruker AXS Inc., Madison, WI, USA, 2001.
3. Sheldrick, G. M. SADABS; University of Göttingen, Göttingen, Germany, 1996
4. SHELXTL version 5.1; Bruker AXS Inc., Madison, WI, USA, 1997.
5. Sheldrick, G. M. CELL_NOW; University of Göttingen, Göttingen, Germany, 2008.
6. Sheldrick, G. M. TWINABS; University of Göttingen, Göttingen, Germany, 2008.